

Epitaxial thin films of pyrochlore iridates: a forward looking approach

Araceli Gutiérrez-Llorente¹

Escuela Superior de Ciencias Experimentales y Tecnología, Universidad Rey Juan Carlos, Madrid 28933, Spain

(*Electronic mail: araceli.gutierrez@urjc.es)

Topological quantum materials that show strongly correlated electrons as well as topological order, for which spin-orbit coupling is a key ingredient, exhibit novel states of matter. One such example is the family of pyrochlore iridates, featuring strong spin-orbital coupling, strong electron interactions as well as geometric frustration, making them an ideal platform to study novel topological phases. High-quality epitaxial pyrochlore iridate films, although challenging to produce, provide a pathway to explore unconventional behaviours and unravel the intrinsic properties of these largely unexplored materials. Additionally, designing interfaces with specific properties is crucial to create multilayered devices that can achieve significant technological breakthroughs using topological states of these materials. This article reviews experimental work on epitaxial pyrochlore iridate thin films, discussing evidence of topological phases found in them. Future research directions are outlined, which include exploring the rich tunability offered by chemical doping, especially when combined with the design of epitaxial heterostructures.

I. INTRODUCTION

Crystalline transition metal oxides (TMO), characterized by strong electron interactions within d -orbitals, are a source of rich physics. These materials can exhibit nearly every known electronic phase.^{1–5} Moreover, remarkable emergent phenomena occur at the interface between different oxides,^{6–16} underscoring their significant potential for integration into electronic devices.^{17–20}

Up to now, extensive research has focused on the broad family of oxides crystallizing in the cubic ABO_3 perovskite structure.²¹ Extending this field of research to oxides with alternative crystal structures remains at the forefront of quantum materials research,^{22–31} opening up an opportunity to reveal exciting and unconventional behaviours in condensed matter physics.

Likewise oxides with perovskite structure, $A_2B_2O_7$ oxides that adopt the pyrochlore structure³² display a wealth of physical properties. These properties include magnetism with exotic ground states (e.g. spin ice),^{33–36} ferroelectricity,³⁷ piezoelectricity,³⁸ superconductivity,^{39–41} colossal magnetoresistance,^{42,43} catalytic activity,^{44–47} ionic conductivity,^{48–51} and high tolerance to radiation damage.^{52,53} This diversity stems partly from the extensive range of possible substitutions at both the A and B sites, akin to perovskites. Yet, this is not the only factor at play.

The pyrochlore crystal structure contains two interpenetrating pyrochlore lattices formed of corner-sharing tetrahedra, each occupied by a different species of cation. Either or both sublattices can host magnetic moments, but the magnetic interactions are frustrated from the geometry, hence failing to develop long-range magnetic order. This geometry is at the origin of a wealth of fascinating phenomena, such as the unconventional anomalous Hall effect driven by spin chirality even without long-range magnetic order of conduction electrons,^{54–57} and fragmentation of the magnetic moment field, in which spin fluctuations coexist with an ordered phase.^{58–62} As a result of the strong frustration, the pyrochlore lattice also hosts fractional quasiparticles (emergent excitations of collective behaviour), for example, emergent mag-

netic monopoles arising from fractionalization of magnetic dipoles in spin ice.^{63–70}

In recent years, the the study of the topology of the electronic structure of crystalline materials has become increasingly central in the research on strongly correlated electron materials. This shift in perspective transcends traditional band theory of crystalline solids, embracing the topological properties (topological invariants) that these energy bands can exhibit,^{71–74} thereby transforming our understanding of matter.

Spin-orbit interaction plays a central role in the emergence of topological phases,^{75–78} intrinsically different from the conventional phases characterized by long-range order and a change in some symmetry. Notably, in $5d$ -transition metal oxides, such as iridium oxides or iridates, the strength of electronic correlation and spin-orbit coupling is of the same order. This makes them ideal candidates for the emergence of topological phenomena, entirely different from those observed in $3d$ -transition metal oxides.^{79–82}

Within this context, the rare-earth pyrochlore iridates $R_2Ir_2O_7$ ($R = Y$ or a lanthanide element) provide a unique opportunity to study the interplay of fundamental interactions, in which Coulomb repulsion among electrons can be tuned by changing the ionic radius of the R cation,^{83–92} and band filling of the Ir $5d$ state can be controlled through doping.^{93,94} Except for $Pr_2Ir_2O_7$, which remains metallic down to the lowest temperature, pyrochlore iridates feature non collinear All-In–All-Out (AIAO) magnetic order for the Ir- $5d$ moment below the metal-insulator transition (MIT), whose temperature decreases with increasing the R ionic radius.⁸³ No evidence of any crystal symmetry change has been found associated with this transition.^{95–97}

All this gives rise to an interesting scenario. For instance, the topological Weyl semimetal phase was first predicted in the pyrochlore iridates.^{17,79,98–100} Although it has not been experimentally achieved yet, experimental signatures of field-induced emergent states, which may be potentially correlated to the predicted topological states were revealed, such as anomalous Hall effect,^{54,101} highly conductive magnetic domain walls in a magnetic insulator,^{102,103} and magnetic field induced MIT.^{91,104,105}

To deeply investigate the fascinating phenomena emerging in these materials and experimentally verify the theoretically predicted properties, it is crucial to grow them as epitaxial films with precise control over crystal growth orientation. This demand arises because magnetic order is highly anisotropic,¹⁰⁶ requiring field-directional studies on single crystals. Moreover, confined geometries result in film properties that are markedly different from those in bulk.^{87,107} Additionally, high-quality epitaxial films are also essential for heterostructure engineering and, ultimately, for the development of devices. However, growth of epitaxial pyrochlore iridate films poses a unique set of challenges.^{108–110}

These challenges encompass the difficulty of achieving stoichiometric compositions in the films due to the high volatility of iridium in oxygen (further details will be provided later),^{111,112} and managing disorder that can significantly impact ground states, hypothetically even fostering new disordered phases in some cases.¹¹³ Hence a strong correlation between the physical properties and the quality of epitaxial pyrochlore oxide films is anticipated, potentially leading to sample-dependent low-temperature experimental outcomes. This interconnection is a hallmark of systems with intricate magneto-structural properties and large ground-state degeneracies, in which the magnetic field (or other external perturbation) can favour one of various competing phases harboured by the material,^{114–116} yet the specific mechanisms remain puzzling.

Furthermore, the scarcity of pyrochlore substrates poses a significant obstacle for experimental studies. This limitation hinders progress, since the ideal substrate share the same structure as the film being grown, thereby determining the epitaxial strain, which greatly impacts the physical properties of the films, as demonstrated within the structural family of perovskites.^{117–119} The wide variety of available single-crystal substrates with cubic and pseudocubic perovskite structures¹²⁰ allows for the tailoring of physical properties in epitaxial perovskite films by tuning strain.^{121,122} In sharp contrast, pyrochlore substrates have only recently become commercially available and remain rare. Consequently, yttria-stabilized ZrO₂ (YSZ) substrate with fluorite structure is the preferred choice for epitaxially growing pyrochlore films, as the pyrochlore structure can be viewed as an ordered defect fluorite with a lattice parameter approximately twice that of YSZ. Nevertheless, this alternative complicates strain engineering in pyrochlore films,^{123–125} making it challenging to explore the tuning of their electronic state topology through lattice strain.

This short review aims to provide a comprehensive overview of experimental studies on epitaxial pyrochlore iridate films, addressing the challenges inherent to this class of materials and briefly discussing future directions for advancing experimental research. Studies on bulk single crystals or polycrystalline films of pyrochlore iridates are excluded in this article, except as references for materials properties. While the primary focus of this review is on experimental work, it also seeks to bridge the gap between tantalizing theoretical predictions and their experimental validation in thin films.

Although this review has limited scope, it is not possible to provide complete reference list. This limitation also applies to the growing number of theoretical studies on topological phases of matter that may be realized in these materials. Readers are referred to several excellent review articles that delve into various related aspects of the subject. Notably, reviews of emergent quantum phases arising from the interplay of strong electron interactions and spin-orbit coupling, illustrated by pyrochlore iridates, were given by Pesin and Balents,⁷⁶ Witczak-Krempa *et al.*,⁷⁷ Savary *et al.*,⁸⁶ Schaffer *et al.*,⁷⁸ Goswami *et al.*,⁹⁰ and Cao and Schlottmann.⁸¹ Moreover, the work by Chakhalian *et al.*¹²⁶ emphasizes the rich possibilities of TMO thin films and heterostructures grown along the [111] direction of perovskite and pyrochlore lattices.

In this paper current state of the field of epitaxial pyrochlore iridate thin films is reviewed. In Section II, the geometrically frustrated lattice structure of pyrochlores is described, since it plays a crucial role in the emerging electromagnetic functions of pyrochlore iridates. Next, section III reviews the magnetic structure of pyrochlore iridates. Section IV discusses research on epitaxial pyrochlore iridate films, and is divided into two subsections about epitaxial growth, in which a survey of deposition methods and specific challenges is presented, and experimental evidence of physical properties of films with emphasis on strain effects. The review closes with an outlook on future directions of research in this field, including chemical doping, and design and growth of epitaxial heterostructures.

II. PYROCHLORE STRUCTURE

The structure of pyrochlore oxides A₂B₂O₆O' (usually written as A₂B₂O₇, cubic *Fd3m*, space group 227) is a geometrically frustrated lattice with four non-equivalent crystallographic positions.^{32,33} This structure comprises two distinct sublattices of A and B sites, which are structurally identical but displaced by half a lattice constant from each other, Fig. 1(a). The ions A and B are located at the vertices of corner-sharing tetrahedra in each sublattice. In the compounds discussed in this paper, A³⁺ represents a rare earth cation, while B⁴⁺ denotes the tetravalent cation of iridium (Ir⁴⁺). The oxygen anions sit at two distinct crystallographic sites, identified as O and O'. The A cations show an eight-fold coordination geometry, with six A-O bonds and two shorter A-O' bonds. The B cations are six-coordinated with oxygen anions, positioned within trigonal antiprisms (BO₆), Fig. 1(b).

The oxygen position parameter x ($0.3125 \leq x \leq 0.375$) controls the position of the O atoms and consequently the coordination geometry around the cations. This parameter describes the trigonal compression of BO₆ octahedra, resulting in regular octahedra around B cations for $x = 0.3125$. For $x = 0.375$ regular cubes form around A cations, which corresponds to a fully disordered material akin to a fluorite lattice, Fig. 1(c). This parameter is highly sensitive to structural disorder.¹²⁷

Along the [111] direction the pyrochlore lattice comprises alternating kagome (the most frustrated 2D geometry for magnetism) and triangular planar layers, which serve as natural cleave planes, Fig. 1(d). Consequently, this direction is ideal

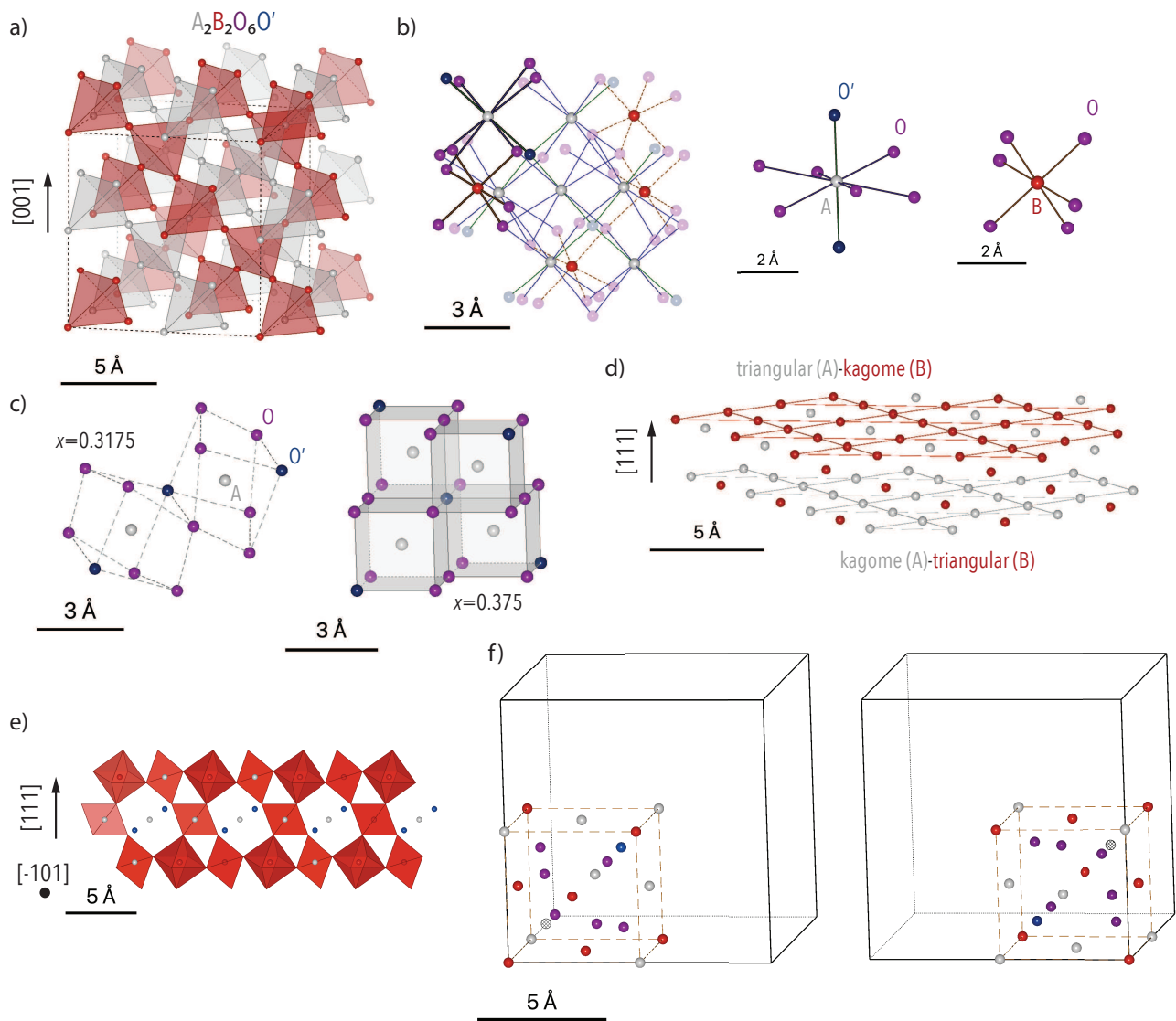


FIG. 1. **Pyrochlore structure.** (a) The pyrochlore lattice $A_2B_2O_6O'$ features two distinct sublattices of A and B sites, with oxygen anions at the tetrahedra vertices are omitted for clarity. (b) The coordination environment of A and B ions: A ions exhibit eight-fold coordination, while B ions show six-fold coordination. A cations are bonded to six O atoms and two O' atoms, with the A- O' bond being shorter than the A-O bond. The O' -A- O' axis is perpendicular to the mean plane of the six O atoms. (c) Coordination around A ions varies with the oxygen position parameter x . (d) Along the $[111]$ direction, the pyrochlore lattice alternates between kagome and triangular planar layers. (e) View along $[-101]$: B ions are in octahedral coordination (corner-linked BO_6 units, with the oxygen atoms at the vertices omitted for clarity) and A_2O' chains fill the interstices. (f) The arrangement of A^{3+} and B^{4+} along (110) results in two types of fluorite subcells within the pyrochlore structure.

for film growth in pyrochlores and is expected to promote the formation of topological phases in oxide thin films.^{87,128,129} Additionally, along the direction $[-101]$ the pyrochlore structure consists of corner-shared BO_6 distorted octahedra with the A cations occupying the interstices, Fig.1(e).

The arrangement of A^{3+} and B^{4+} ions along the direction $[110]$ defines two types of fluorite subcells within the pyrochlore lattice, Fig.1(f). Thus, the pyrochlore structure can also be described as a superstructure composed of eight nearly identical fluorite subunits, with intrinsic ordered oxygen vacancies at $1/8$ of the oxygen sites to maintain charge neutral-

ity.

The pyrochlore lattice exhibits a strong tendency towards disorder at both cation and oxygen sites. This disorder can be induced by substitution of A cations by B ones, with simultaneous rearrangements in both sublattices, or by the randomisation of oxygen vacancies, through the migration of oxygen to the nearest vacant site.^{127,130,131} Eventually, the pyrochlore can transform into a disordered fluorite structure by mixing the A and B ions within the cation sublattices and randomly distributing the oxygen vacancies. This predisposition to disorder is more pronounced in compounds with small A

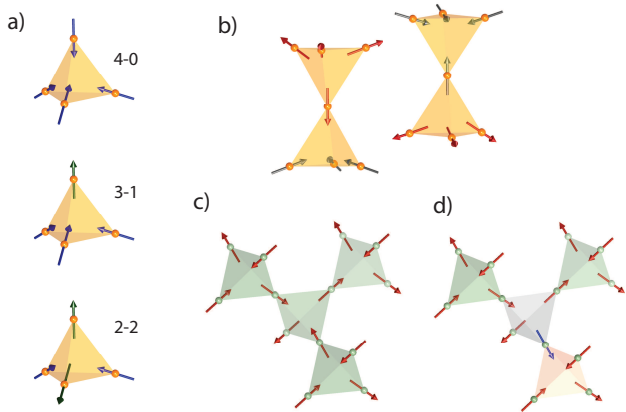


FIG. 2. **Magnetic ions in the pyrochlore lattice.** (a) Different arrangements of spins in a single tetrahedron with $\langle 111 \rangle$ Ising anisotropy. Spins align along the local direction from a vertex to the center of the tetrahedron in a configuration that can be 4-0, with the four spins pointing in; 3-in 1-out; or, 2-in 2- out. (b) Two distinct magnetic domains All-in-All-out/All-out-All-in of the 4-0 configuration. (c) Spin ice state in a pyrochlore lattice in which each tetrahedron has the 2-2 configuration. In this case, a single spin flip (d) produces elementary excitations on two neighbouring tetrahedra that can be regarded as fractionalized magnetic monopoles.

cations and large B cations.¹³⁰ Additionally, lattice displacements and local off-centering of the A and O ions were also reported.^{132,133}

It is well established that weak disorder can lead to spin-glassy behaviour in pyrochlore magnetic oxides.^{134,135} Interestingly, rather than yielding glassy behaviour, it was suggested that weak disorder introduced by structural imperfections around the magnetic sites in non-Kramers ions (such as Pr^{3+} or Tb^{3+}) of pyrochlore magnetic oxides can give rise to a quantum spin liquid ground state.¹¹³ To test this hypothesis, experimental studies^{136,137} on $\text{Pr}_2\text{Zr}_2\text{O}_7$ focused on diffuse neutron scattering experiments around Bragg peaks caused by structural distortions. These experiments revealed a level of disorder undetectable by conventional diffraction, but sufficient to induce quantum fluctuations in spin. However, a quantum spin liquid state induced by disorder has yet to be experimentally confirmed.¹³⁸ In this context, it is noteworthy that local atomic arrangements in disordered crystalline materials can be nonrandom, giving rise to short-range order at a length scale shorter than the unit cell.¹³⁹ The impact of this short-range order on physical properties remains to be fully understood.

III. MAGNETIC ORDER/ STRUCTURE IN PYROCHLORE IRIDATES

Except for $\text{Pr}_2\text{Ir}_2\text{O}_7$, which remains magnetically disordered in a metallic state down to the lowest temperatures,^{140,141} pyrochlore iridates exhibit antiferromagnetism below the metal-to-insulator transition. This

transition is characterized by a non collinear All-In-All-Out (AIAO) ordering of the Ir^{4+} sublattice in the magnetic insulating phase. The AIAO configuration can transform into a 2-2 or 3-1 structure when a magnetic field is applied along specific crystal axis, significantly affecting the magnetic and electronic properties of the material, Fig.2. This non-coplanar spin arrangement is at the origin of the spin-chirality induced anomalous Hall effect.¹⁴² Moreover, nontrivial topological electronic bands, closely related to this magnetic order, have been predicted.^{79,88,90,143–146}

There is experimental evidence of the AIAO magnetic arrangement in the iridium sublattice in $\text{Nd}_2\text{Ir}_2\text{O}_7$,^{105,147–149} $\text{Eu}_2\text{Ir}_2\text{O}_7$,^{150–152} $\text{Tb}_2\text{Ir}_2\text{O}_7$,^{153–155} $\text{Er}_2\text{Ir}_2\text{O}_7$,¹⁵³ $\text{Sm}_2\text{Ir}_2\text{O}_7$,^{148,156} $\text{Yb}_2\text{Ir}_2\text{O}_7$ and $\text{Lu}_2\text{Ir}_2\text{O}_7$.¹⁵⁷

Although the magnetic domains are antiferromagnetic, their alignment can be controlled through a magnetic field cooling procedure. And the magnetic domain structure can be detected through magnetotransport measurements, as spin-orbit coupling renders conduction electrons responsive to the local spin arrangement. For example, magnetic-field induced AIAO/AOAI domain inversion has been reported in epitaxial films of $\text{Eu}_2\text{Ir}_2\text{O}_7$ depending on the polarity of the cooling magnetic field in the $[111]$ crystallographic direction^{151,158} (see section IV B).

The rare-earth cation sublattice can also be magnetic in rare-earth pyrochlores, leading to even more complex magnetic structures. The f -electrons of the rare-earth R^{3+} ion can carry a net magnetic moment in a Kramers doublet ($\text{R} = \text{Nd}, \text{Sm}, \text{Gd}, \text{Dy}, \text{Yb}$) or a non-Kramers doublet ($\text{Pr}, \text{Tb}, \text{Ho}$). The f - d exchange interaction between the localized $\text{R}4f$ electron moments and the more itinerant $\text{Ir}5d$ electrons results in the modulation of the magnetic order of Ir^{4+} moments by the molecular fields of R^{3+} magnetic ions (Fig.3). Theoretical studies suggested that this exchange interaction between Ir and R ions is crucial for stabilizing topological phases in pyrochlore iridates, such as the Weyl semimetal and the axion insulator.⁸⁵

For example, in polycrystalline samples of $\text{Tb}_2\text{Ir}_2\text{O}_7$, the Ir molecular field induces the ordering of Tb magnetic moments below 40 K into an AIAO magnetic arrangement, while no evidence of magnetic long-range order was observed in the Er sublattice of $\text{Er}_2\text{Ir}_2\text{O}_7$ down to 0.6 K.¹⁵³ This different behaviour was attributed to the anisotropy of the R site. The molecular fields from Ir^{4+} in the AIAO order induce the Tb^{3+} moments to adopt a AIAO configuration at low temperature due to their strong axial magnetocrystalline anisotropy along the $\langle 111 \rangle$ direction. In contrast, Er exhibits easy-plane anisotropy, with its magnetic moments perpendicularly oriented to the Ir molecular field.

$\text{Nd}4f$ moments also develop the AIAO-type ordering at lower temperature due to f - d exchange coupling in $\text{Nd}_2\text{Ir}_2\text{O}_7$.^{149,159} The onset temperature of the AIAO-type magnetic ordering of the $\text{Ir}5d$ moment is 15 K, and domain flipping between the 4-0 and 0-4 configuration is driven by a magnetic field along $[111]$. At 2 K, a magnetic field $H \parallel [111]$ modulated by f - d exchange coupling can switch between the two variants AIAO/AOAI in the $\text{Ir}5d$ configuration and from 0-4 to 3-1 in the $\text{Nd}4f$ configuration as H increases. In con-

trast, both Nd and Ir sublattices develop a 2-2 out configuration under a magnetic field $H \parallel [001]$.¹⁴⁹

$\text{Gd}_2\text{Ir}_2\text{O}_7$ and $\text{Ho}_2\text{Ir}_2\text{O}_7$ exhibit complex magnetic order patterns. The ordering temperature of the Ir^{4+} sublattice in an AIAO structure, which coincides with the metal-to-insulator transition, is approximately 127 K and 140 K for polycrystalline samples of $\text{Gd}_2\text{Ir}_2\text{O}_7$ and $\text{Ho}_2\text{Ir}_2\text{O}_7$, respectively. The ordering temperatures for Gd^{3+} and Ho^{3+} are around 50 K (induced by the AIAO Ir molecular field through Ir—Gd magnetic coupling) and 18 K, respectively.^{61,160}

$\text{Gd}_2\text{Ir}_2\text{O}_7$ and $\text{Ho}_2\text{Ir}_2\text{O}_7$ display different types of anisotropy. Gd^{3+} in $\text{Gd}_2\text{Ir}_2\text{O}_7$ does not exhibit strong single-ion anisotropy, although a weak easy-plane anisotropy for Gd^{3+} emerges below 2 K, owing to the mixing of its ground state with higher spectral multiplets, that can result in anisotropic exchange.¹⁶⁰ Ho^{3+} in $\text{Ho}_2\text{Ir}_2\text{O}_7$ shows an easy-axis anisotropy along the $[111]$ direction and fragmentation of the magnetisation below 2 K into two distinct components.⁶¹ an ordered antiferromagnetic phase and a disordered Coulomb phase with ferromagnetic correlations.⁵⁸ Quantitative analysis of the interplay between the molecular fields of the AIAO ordered Ir sublattice and an external magnetic field on experimental data from polycrystalline samples is challenging, but Monte Carlo simulations carried out to elucidate the underlying physics of the unconventional magnetic ground state indicate that applying an external magnetic field applied along different directions can induce the stabilization of exotic phases, such as fragmented kagome ice state, characterize by fragmented phases in the kagome planes and spins aligned along the magnetic field in the triangular planes. On the other hand, experimental measurements on single crystals of $\text{Ho}_2\text{Ir}_2\text{O}_7$ combined with Monte Carlo simulations indicate that an applied magnetic field along the direction $[111]$ arranges the Ho moments into a 3-1 configuration, favouring one type of configuration of AIAO domains in Ir (conversely, applying the field in the opposite direction favours the alternate configuration in the Ir sublattice). In contrast, applying the magnetic field along $[100]$ orders the Ho spins into a 2-2 state.¹⁶¹

Fragmentation of magnetic moments between disordered and ordered components was also observed in $\text{Dy}_2\text{Ir}_2\text{O}_7$. Experimental measurements of polycrystalline and single crystal samples of $\text{Dy}_2\text{Ir}_2\text{O}_7$ show that it stabilizes the fragmented monopole crystal state, in which antiferromagnetic AIAO order coexists with a Coulomb phase spin liquid, at temperatures below around 1 K.¹⁶²

Geometrically frustrated magnets are known to have strong spin-phonon coupling.^{163–165} In 5d materials, such as the pyrochlore iridates, the Dzyaloshinskii-Moriya (DM) interaction, which originates from spin-orbit coupling, may induce spin-phonon coupling.¹⁶⁶

Strong spin-phonon coupling has been reported in polycrystalline samples of the pyrochlore iridate $\text{Y}_2\text{Ir}_2\text{O}_7$ by infrared spectroscopy and first-principles calculations.¹⁶⁶ Some Ir-active phonons soften and sharpen below the antiferromagnetic ordering temperature at 170 K. Since the AIAO magnetic ordering in pyrochlore iridates is not accompanied by structural transitions, the observed phonon anomalies must be due to the coupling to the AIAO magnetic order. The authors

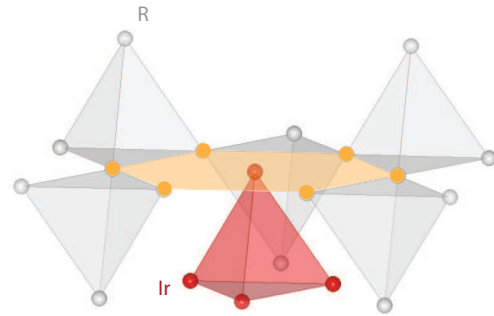


FIG. 3. **R 4f—Ir 5d exchange coupling in $\text{R}_2\text{Ir}_2\text{O}_7$.** If the ion R^{3+} carry a magnetic moment, the application of an external magnetic field can control the R spin configuration which, in turn, modulates the Ir magnetic ordering. A single Ir^{4+} ion (red) is surrounded by six nearest-neighbouring R-4 sites (yellow) whose moments generate an effective magnetic field at the Ir site. Moreover, below the metal-insulator transition temperature, when the Ir^{4+} sublattice orders in the AIAO phase, a magnetic field oriented along the local $[111]$ directions on the R^{3+} sublattice is generated.

attributed these anomalies to the modulation of the Ir—O—Ir bond angle by the DM interaction.

Furthermore, Ueda *et al.*¹⁶⁷ studied $\text{Eu}_2\text{Ir}_2\text{O}_7$ using Raman scattering. Their research unveiled large phonon anomalies triggered by the emergence of magnetic AIAO order in $\text{Eu}_2\text{Ir}_2\text{O}_7$, below 115 K. Notably, Ir—O—Ir bond bending vibration exhibited line-shape anomalies at the magnetic phase transition, indicating strong electron-phonon interactions that are crucial for understanding the magnetic ordering behaviours of pyrochlore iridates. The authors proposed a spin-phonon coupling mechanism modulated by exchange interactions, widely accepted for 3d materials; phonon-induced modulation of the orbitals, which affects magnetism via spin-orbit coupling; and electron-phonon coupling through charge fluctuations. However, the microscopic mechanism responsible for the electron-phonon interactions that the experimental data reveal remains unresolved.

Coupling of phonons to spins has also been studied in $\text{Pr}_2\text{Ir}_2\text{O}_7$ by thermal transport measurements in single crystals.¹⁶⁸ A strong resonant scattering between phonons and paramagnetic spins was found, hindering longitudinal heat conduction.

IV. EPITAXIAL PYROCHLORE IRIDATE FILMS

A. Epitaxial growth

Translating the physical properties of bulk materials into high-quality epitaxial films presents significant challenges due to the formation of intrinsic defects. These include point defects, which accommodate structural imperfections and non-stoichiometry, and strain-relieving misfit dislocations, both of which can degrade film properties.^{110,185} The level of difficulty varies for each system, but overcoming these challenges is highly rewarding, as dimensional confinement and interface

TABLE I. Single-crystal pyrochlore iridate films synthesized up to date.

Material Substrate	Growth process
Pr ₂ Ir ₂ O ₇ YSZ(111)	<ul style="list-style-type: none"> • SPE:^a PLD (Ir-rich target Pr:Ir=1:2, RT,^b 10 mTorr, 0.65 Jcm⁻², 5 Hz), post-annealing at 1000°C, 1.5 h in air.^{123,169} Conventional PLD at 10 mTorr, 0.65 Jcm⁻², 5 Hz, T up to 800°C, using stoichiometric and Ir-rich (Pr:Ir=1:2) targets, results in insulating films, consistent with Pr₂O₃ phase instead of metallic Pr₂Ir₂O₇.¹⁶⁹ • SPE: RF sputtering (polycrystalline Pr₂Ir₂O₇ target, RT, 15 mTorr in Ar:O₂=90:10), post-annealing at 800°C, 12 h in air.¹²⁴ • Partially strained films. First step: RRHSE.^c Alternate Pr₂Ir₂O₇ and IrO₂ amorphous layers in each cycle by PLD at 600°C, 50 mTorr, 1.5 Jcm⁻², 5 Hz. Then the temperature is increased to 800°C for 30 s, and rapidly decreased to 600°C for the next cycle. Second step: post-annealing at 1000°C in a sealed tube with IrO₂ powder for 1 h.¹⁷⁰ • Experimental and computational study of <i>in situ</i> phase formation in the Pr-Ir-O₂ system. Co-sputtering deposition: the flux of Pr₂Ir₂O₇ and IrO₂ is controlled separately.¹⁷¹ Pr₂Ir₂O₇ can only form high-quality crystals with $T > 1073$ K and $P_{O_2} > 9$ Torr.
Nd ₂ Ir ₂ O ₇ YSZ(111)	<ul style="list-style-type: none"> • SPE: RF sputtering (RT, 12.5 mTorr in Ar:O₂=99:1), post-annealing at 750°C, for 12 h, with oxygen partial pressure between 30 mbar and 200 bar. Annealing at $\geq 775^\circ\text{C}$ results in the formation of impurity phases.¹⁷² • SPE: PLD (600°C, 50 mTorr, 4.5 Jcm⁻² and 3 Hz), post-annealing at 1000°C, 1 h in air.¹⁷³ • Strained films.^{125,174,175} RRHSE. Stoichiometric amorphous Nd₂Ir₂O₇ and IrO₂ deposited by PLD at 600°C, 50 mTorr, 5 Hz and 4.5 Jcm⁻² (ref.¹²⁵) or 1.7 Jcm⁻² (ref.¹⁷⁴). Then, rapid thermal annealing, T up to 800°C (ref.¹²⁵) or 850°C (ref.¹⁷⁴) at 400°C/min⁻¹. Processes monitored by RHEED^d, alternatively repeated until desired film thickness. • Relaxed films. SPE: PLD at $T \leq 600^\circ\text{C}$, followed by annealing at $T \geq 800^\circ\text{C}$ in a sealed tube with IrO₂ powder in air.¹²⁵ • SPE: PLD (550°C, 50 mTorr, 1.1 Jcm⁻², 5 Hz), post-annealing at 1000°C, 1.5 h in air.¹⁷⁶
Eu ₂ Ir ₂ O ₇ YSZ(111)	<ul style="list-style-type: none"> • SPE: PLD (Ir-rich target: Eu:Ir=1:3, 500°C, 100 mTorr Ar gas containing 1% O₂, 6 Jcm⁻² and 10 Hz), post-annealing at 1000°C, 1.5 h in air.^{151,154} • SPE:¹⁷⁷ same conditions as in Y₂Ir₂O₇ (Ref.¹⁷⁸). • SPE: PLD (Ir-rich target: Eu:Ir=1:3, 550°C, 50 mTorr, 1.1 Jcm⁻² and 5 Hz), post-annealing at 1000°C, 1.5 h in air with IrO₂ powder.¹⁷⁹⁻¹⁸¹ • SPE: PLD, alternate ablation of IrO₂ and Eu₂O₃ targets at substrate temperature in the range 450-550°C and oxygen pressure 20-40 mTorr. Post-annealing in air for a few hours with annealing temperature from 800 to 1200°C.¹⁸²
Tb ₂ Ir ₂ O ₇ YSZ(111)	<ul style="list-style-type: none"> • SPE:^{183,184} same conditions as in Eu₂Ir₂O₇ (Ref.^{151,154}).
Dy ₂ Ir ₂ O ₇ YSZ(111)	<ul style="list-style-type: none"> • SPE: PLD, target with precursors at a ratio of 3:1=Ir:Dy, laser fluence of 1.5 Jcm⁻², 3 Hz, substrate temperature fixed at 650°C, and oxygen pressure of 0.05 mbar during the deposition. Post-annealing ex-situ at 1000°C for 1.5 h.
Y ₂ Ir ₂ O ₇ YSZ(111)	<ul style="list-style-type: none"> • SPE: PLD (Ir-rich target: Y:Ir=1:3, 480-520°C, 50-100 mTorr Ar:O₂=10:1, 6 Jcm⁻² and 10 Hz), post-annealing at 1000°C for 2 h in air or at 900-950°C for 8-10 min under 650 Torr atmosphere of O₂ inside the deposition chamber.¹⁷⁸

^a Solid-phase epitaxy.^b RT: Room temperature.^c RRHSE: Repeated rapid high-temperature synthesis epitaxy. See also Fig. 5.^d RHEED: Reflection high-energy electron diffraction.

effects can enhance or induce certain material properties that are not observed in bulk materials.

Common thin film synthesis approaches for growing crystalline oxide films^{107,186,187} include pulsed laser deposition (PLD),¹⁸⁸⁻¹⁹⁰ sputtering,¹⁹¹ and molecular beam epitaxy (MBE).¹⁹²⁻¹⁹⁴ In these physical vapour deposition (PVD) methods, the oxygen partial pressure and substrate temperature define the thermodynamic window for the growth of dif-

ferent materials and are crucial in determining the phases that form in the film.

Growing high-quality single crystalline films of pyrochlore iridates needs both high temperatures and high oxygen partial pressure, as iridium is hard to oxidize. At these elevated temperatures, iridium metal, known for its highly volatility in oxygen, forms the volatile oxide IrO₃.^{111,195} This high vapour pressure of IrO₃ is the primary challenge related to

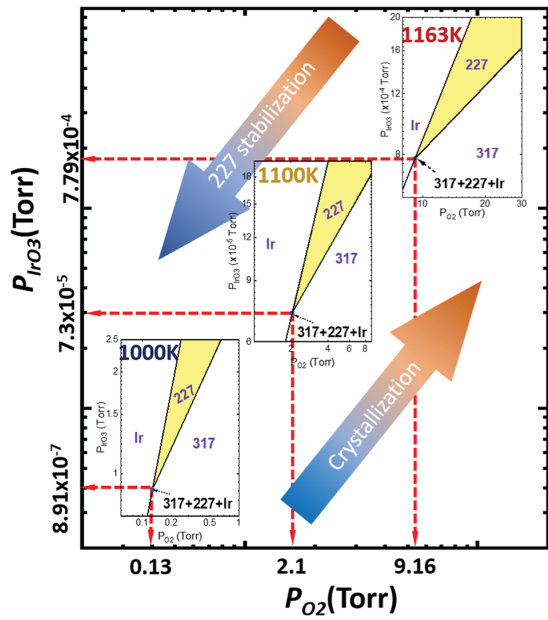


FIG. 4. Calculated phase diagram of the system $\text{Pr-PrO}_3\text{-O}_2$ at 1000, 1100 and 1163 K. According to calculations, partial pressure P_{IrO_3} for the formation of $\text{Pr}_2\text{Ir}_2\text{O}_7$ decreases three orders of magnitude and P_{O_2} decreases by 70 times when temperature goes from 1163 K down to 1000 K. However, films deposited *in situ* at temperatures lower than 1073 K exhibited low quality. L. Guo *et al.*, npj Computational Materials, 7(1), 10.1038/s41524-021-00610-9, 2021; licensed under a Creative Commons Attribution (CC BY) license.¹⁷¹

Ir oxidation.¹⁹⁶ IrO_3 gas is pumped away from the vacuum chamber, resulting in the depletion of Ir in the deposited films. Consequently, *in situ* growth of pyrochlore iridates by PLD^{151,169} and sputtering¹⁷¹ have been hindered.

For instance, PLD carried out to grow $\text{Eu}_2\text{Ir}_2\text{O}_7$ films at temperatures in the range 1000-1250°C and oxygen partial pressure between $10^{-7} - 10^{-1}$ Torr results in the crystallisation of metallic Ir and polycrystalline Eu_2O_3 . Increasing the pressure up to 1 Torr at the same temperature range leads to the evaporation of Ir and the formation of crystalline Eu_2O_3 only.¹⁵¹ Additionally, using an Ir-rich target¹⁶⁹ or a separate IrO_2 target¹⁷¹ does not overcome these difficulties for *in situ* PLD growth of pyrochlore iridates.

Perovskite-related phases of iridates, such as SrIrO_3 and Sr_2IrO_4 , along with the binary oxide IrO_2 , have been successfully grown using MBE.¹⁹⁷ Recently, this method was also employed to grow a pyrochlore titanate.¹⁹⁸ However, MBE has yet to be reported for the growth of pyrochlore iridates.

Guo *et al.*¹⁷¹ carried out computational calculations and experimental growths in the Pr-Ir-O_2 system by simultaneous sputtering from both $\text{Pr}_2\text{Ir}_2\text{O}_7$ and IrO_2 targets. They also found that *in-situ* synthesis of $\text{Pr}_2\text{Ir}_2\text{O}_7$ at high temperature (1163 K) needs oxygen partial pressures ≥ 9 Torr, making it unfeasible in PVD systems, Fig.4. $\text{Pr}_2\text{Ir}_2\text{O}_7$ can only form if both partial pressures of gas species O_2 and $\text{IrO}_3(\text{g})$ are high, otherwise Ir(s) forms at low oxygen partial pressures. Moreover, lower growth temperature (1073 K), which would allow for lower partial pressures, resulted in films with poor crys-

tallinity.

Kim *et al.*¹⁹⁹ studied the chemical kinetic instabilities of IrO_2 thin films, by *in-operando* spectroscopic ellipsometry. They found that conventional *in-situ* growth techniques are inadequate for growing pyrochlore iridate thin films. This is due to the unavoidable dissociation of IrO_2 and formation of $\text{IrO}_3(\text{g})$ at high temperatures, while crystallization of the film is not possible at lower temperatures.

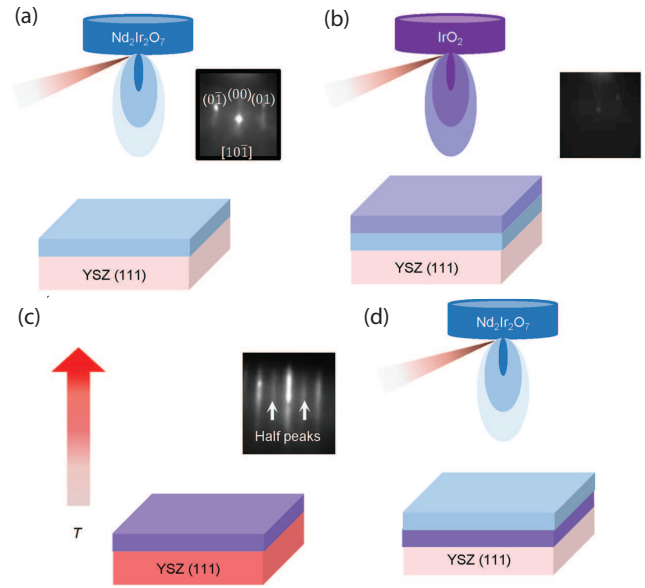


FIG. 5. Steps of the Repeated Rapid High Temperature Synthesis Epitaxy (RRHSE) method for growing $\text{Nd}_2\text{Ir}_2\text{O}_7$ thin films. (a) Conventional PLD of a $\text{Nd}_2\text{Ir}_2\text{O}_7$ target at 600°C and oxygen partial pressure of 50 mTorr. (b) Conventional PLD of an IrO_2 target to compensate for Ir loss. (c) Rapid thermal annealing for approximately 30 s, heating up to 850°C at a rate of 400°C/min. (d) Repeat steps (a) to (c) until the desired thickness of the film is achieved. J. K. Song *et al.*, APL Materials, 11(6), 10.1063/5.0153164, 2023; licensed under a Creative Commons Attribution (CC BY) license.¹⁷⁴

To address these challenges of epitaxial growth techniques for pyrochlore iridates, the synthesis is divided into two steps using the solid-state epitaxy method. First, a layer with the correct Ir stoichiometry is formed, followed by its crystallisation.^{108,109,200} In this approach, an amorphous layer, grown at a much lower temperature than needed for epitaxial growth, transforms into an epitaxial thin film through a high temperature post-annealing process, with the single crystal substrate serving as a seed. The amorphous thin films, which serve as precursors for crystallization, are formed by PLD or sputtering.

An alternative approach is called repeated rapid high-temperature synthesis epitaxy (RRHSE, Fig. 5).^{125,174,175} This method involves a rapid thermal annealing, performed *in situ*. The amorphous layer formed from the PLD previous step at low temperature (approximately 600°C) is heated up to 850°C at a rate of 400°C/min for about 30 s using an infrared laser heater in the deposition chamber. Then the temperature is then reduced to 600°C for a new cycle of ablation followed by a rapid thermal annealing. In this synthesis process, as the

annealing is carried out under pumping of $\text{IrO}_3(\text{g})$, the Ir loss is compensated by ablating an IrO_2 target before the annealing step. In contrast to the standard solid-state epitaxy approach, which results in relaxed films, RRHSE enables the growth of strained films.

Table I provides a detailed summary of the epitaxial pyrochlore iridate films synthesized to date.

Another critical issue in synthesising pyrochlore iridate films is that even minute variations in the ratio of the rare-earth element to iridium can significantly impact their electronic and magnetic properties. Cation disorder, in which an excess of rare-earth ions occupies the Ir sites in $\text{R}_{2+x}\text{Ir}_{2-x}\text{O}_{7-x/2}$, commonly referred to as *stuffing*, can bring about substantial changes in the ground state properties of these materials. For instance, the ground state of $\text{Pr}_2\text{Ir}_2\text{O}_7$ is still under discussion, due to the difficulty in achieving the correct stoichiometry, even in polycrystalline samples.²⁰¹ Experimental results for polycrystalline $\text{Eu}_2\text{Ir}_2\text{O}_7$ were also found to depend on the synthesis parameters. Specifically, deviations from the ideal Eu/Ir ratio increased the variability in its metallic behaviour above the metal-to-insulator transition.²⁰² Moreover, the ordering temperature of a single crystal of $\text{Tb}_2\text{Ir}_2\text{O}_7$ decreased from 130 K in the stoichiometric material to ~ 71 K with an excess of Tb of 0.18, although it retained the AIAO magnetic structure.¹⁵⁵ Strong sample dependence of the magnetotransport properties was also found in single crystals of $\text{Pr}_2\text{Ir}_2\text{O}_7$. Minor antisite mixing between Pr and Ir resulted in local structural imperfections that influence the Ir 5d topological electronic band, which is modulated by the interaction between Ir conduction electrons and localized Pr 4f moments. Therefore, a precise structural analysis was conducted to select a near-stoichiometric sample.²⁰³

B. Experimental findings in epitaxial pyrochlore iridate films

The investigation of fundamental effects in pyrochlore iridates in thin film form raises many interesting questions and is still in its early stages. Current research has primarily focused on the magnetic Weyl semimetal state and its associated topological phenomena, such as the anomalous Hall effect and negative magnetoresistance that can provide evidence for the chiral anomaly (charge transfer between Weyl fermions with opposite chirality).

$\text{Pr}_2\text{Ir}_2\text{O}_7$ thin films, grown via solid-state epitaxy, show topological nontrivial transport properties.¹²³ Certain regions of the $\text{Pr}_2\text{Ir}_2\text{O}_7$ film are stained to the substrate, as indicated by scanning transmission electron microscopy, breaking the cubic symmetry due to epitaxial compressive strain in the in-plane direction (tensile strain along the surface normal [111] direction), and exhibiting spontaneous Hall effect under zero magnetic field. The Hall resistivity increases with decreasing temperature from 50 K down to 700 mK without any observable spontaneous magnetization. This observation is consistent with the emergence of the magnetic Weyl semimetal phase. The authors attributed the breaking of time-reversal symmetry, necessary for the appearance of a Weyl semimetal phase, to the magnetic order of Ir 5d electrons, although this

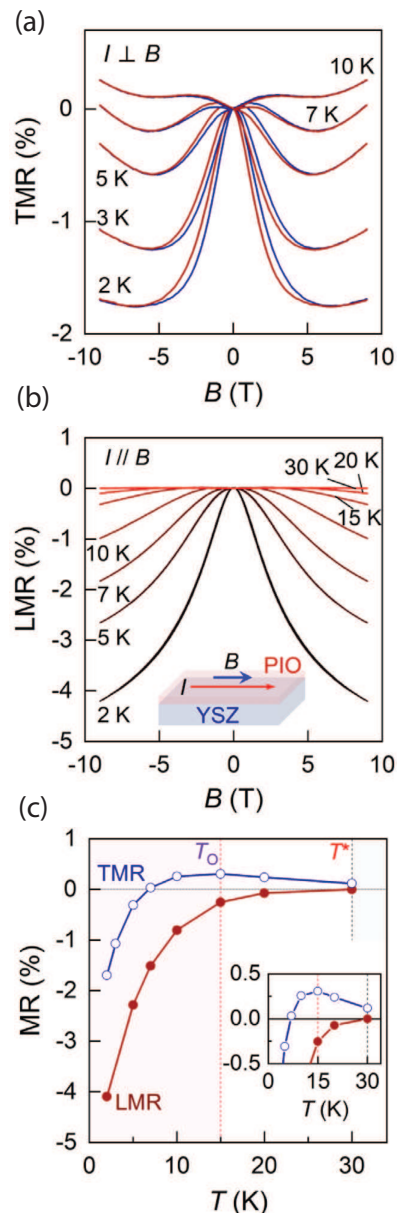


FIG. 6. **Magnetotransport in strained $\text{Pr}_2\text{Ir}_2\text{O}_7$ films.** (a) Transverse magnetoresistance (TMR) at different temperatures. Blue (red) lines correspond to field decreasing (increasing) magnetic field sweeps. (b) Longitudinal magnetoresistance (LMR) as a function of temperature. (c) TMR and LMR measured as 9 T as a function of temperature. Y. Li *et al.*, *Advanced Materials*, 33(25), 10.1002/adma.202008528, 2021; licensed under a Creative Commons Attribution (CC BY) license.¹⁷⁰

point is unsettled.¹²⁴ Additionally, the Weyl semimetal phase can be induced by a magnetic field collinear to the electric current, giving rise to negative longitudinal magnetoresistance, arising from the chiral anomaly.⁹⁹

Guo *et al.* observed an increase in the onset temperature of the spontaneous Hall effect by one order of magnitude in epitaxial films of $\text{Pr}_2\text{Ir}_2\text{O}_7$ compared to the bulk material, from 1.5 K to 15 K.¹²⁴ This effect likely arises from the topolog-

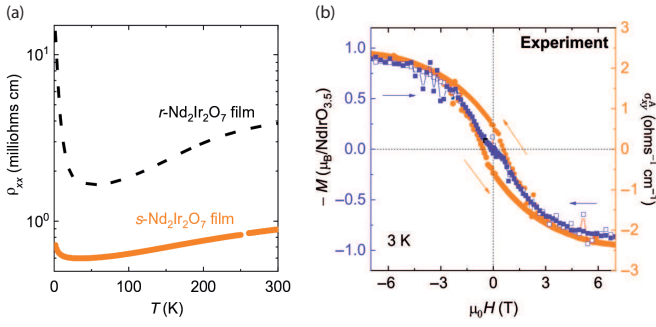


FIG. 7. Transport properties of strained $\text{Nd}_2\text{Ir}_2\text{O}_7$ thin films. (a) Longitudinal resistivity ρ_{xx} as a function of temperature for a fully strained $\text{Nd}_2\text{Ir}_2\text{O}_7$ film (orange). ρ_{xx} for a relaxed film is also shown (dashed, black). (b) Magnetization (M , blue) and anomalous Hall conductivity (σ_{xy}^A , orange) of a strained film with the current along $[\bar{1}10]$ and magnetic field applied along $[111]$. The anomalous Hall conductivity was calculated as $\sigma_{xy}^A = \rho_{xy}^A / ((\rho_{xx})^2 + (\rho_{xy}^A)^2)$, where the anomalous Hall resistivity ρ_{xy}^A is derived from the measured Hall resistivity ρ_{xy} after antisymmetrizing using positive and negative field sweep branches and removing the linear part, corresponding to the conventional Hall resistivity. W. J. Kim *et al.*, Science Advances, 7(29), 10.1126/sciadv.abb1539, 2020; licensed under a Creative Commons Attribution (CC BY) license.¹²⁵

ical Hall effect, in which time-reversal symmetry is broken from the frustrated spin-liquid correlations rather than a net magnetic moment. A minute lattice distortion of the Ir sublattice, caused by epitaxial strain, localizes the Ir moments although no sign of long-range AIAO order is observed. Thus, two hypotheses are proposed as the origin of the time-reversal symmetry breaking in these films: Ir-site spin correlations or a modification of the Pr-Pr coupling through spin polarization at the Ir site. Further investigation of the magnetism in these epitaxial films is needed.

While AIAO magnetic order is not observed in unstrained bulk or single crystals of $\text{Pr}_2\text{Ir}_2\text{O}_7$, mean-field calculations for $\text{Pr}_2\text{Ir}_2\text{O}_7$ under biaxial strain, based on the Hubbard model predict a strain-induced AIAO antiferromagnetic order in $\text{Pr}_2\text{Ir}_2\text{O}_7$ films with small strain ($< 0.3\%$) that breaks time-reversal symmetry, leading to a WSM phase.¹⁷⁰ To test this prediction, films with a strain of $\approx 0.2\%$ were synthesised. These films exhibit negative transverse magnetoresistance (TMR) with a hysteresis feature below 15 K when magnetic field is applied along the $[111]$ direction (Fig. 6(a)), contrasting with the positive TMR observed in bulk $\text{Pr}_2\text{Ir}_2\text{O}_7$. The contribution of the AIAO magnetic ordering is dominant below 7 K, with coexistence of paramagnetic and AIAO phases in the range of 7–15 K. The hysteresis behaviour is consistent with the presence of two degenerate magnetic domains in the AIAO antiferromagnetic state, although the AIAO ordering was not confirmed by other techniques. Negative longitudinal magnetoresistance without hysteresis is observed below 30 K (Fig. 6(b)), which is attributed to the chiral anomaly of Weyl fermions in the WSM phase, once the influence of current jettisoning on longitudinal resistivity measurements is ruled out.

Empirical evidence supporting topological phenomena has also been observed in antiferromagnetic $\text{Nd}_2\text{Ir}_2\text{O}_7$ films.¹²⁵ A

significantly larger anomalous Hall conductivity was found in compressively strained $\text{Nd}_2\text{Ir}_2\text{O}_7$ films compared to relaxed films, suggesting that biaxial strain affects the Berry curvature. The AIAO spin structure of the Ir sublattice is modulated under strain, leading to the formation of magnetic multipoles that can induce anomalous Hall effect (AHE) without magnetization. The authors applied the theoretical framework of atomic cluster multipoles in antiferromagnetic crystals, as proposed by Suzuki *et al.*,²⁰⁴ to the noncollinear magnetic structure of $\text{Nd}_2\text{Ir}_2\text{O}_7$ films. It is suggested that octupoles moments with the same symmetry as magnetic dipole moments can induce AHE without magnetization. These multipoles form under strain but not in relaxed films, which exhibit negligible spontaneous Hall conductivity.

More recently, a linear scaling between saturated anomalous Hall conductivity at 9 T and Hall carrier density was found in strained $\text{Nd}_2\text{Ir}_2\text{O}_7$.¹⁷⁵ This linear slope changes its sign around the ordering temperature of Nd moments. This hump-like feature was attributed to a change of the energy levels of Weyl nodes, according to numerical calculations under epitaxial strain that breaks the cubic symmetry.

The conductivity of domain walls (DW) in $\text{Nd}_2\text{Ir}_2\text{O}_7$ single crystals has been experimentally found to be one order of magnitude higher than in the bulk material.^{105,149} DW-induced magnetotransport in $\text{Nd}_2\text{Ir}_2\text{O}_7$ films has also been investigated.¹⁷³ In these films, AHE from both bulk and DW has been reported under an applied magnetic field along the $[111]$ direction, which is expected to favour the formation of DW within the (111) plane. It is proposed that hysteretic, hump-like behaviour of AHE observed in these films originates from DW conduction.

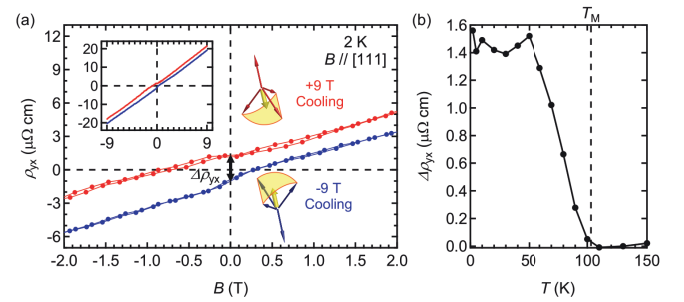


FIG. 8. Hall resistivity in $\text{Eu}_2\text{Ir}_2\text{O}_7$ single crystalline thin films. (a) Field cooling at +9 T or -9 T is applied, giving rise to A or B domains of the AIAO spin structure. The Hall resistance exhibits a non-zero value at 0 T, $\Delta\rho_{xy}$. (b) Temperature dependence of $\Delta\rho_{xy}$ (dashed line at the transition temperature). T. C. Fujita *et al.*, Scientific Reports, 5, 10.1038/srep09711, 2015; licensed under a Creative Commons Attribution (CC BY) license.¹⁵¹

In epitaxial films of $\text{Eu}_2\text{Ir}_2\text{O}_7$, it was found that the magnetic domain structure (AIAO or AOAI) can be selectively stabilized by the polarity of the cooling field along the $[111]$ direction above ± 3 T (a multidomain structure is formed by cooling in lower magnetic fields).¹⁵¹ The domain structure formed in this way remains robust against a magnetic field of at least 9 T below the temperature at which the metal-to-insulator transition occurs. These robustness in $\text{Eu}_2\text{Ir}_2\text{O}_7$ has

been attributed to the nonmagnetic character of Eu^{3+} . As conduction electrons are sensitive to the local spin structure due to spin-orbit coupling, the magnetic domain structure was detected by magnetotransport measurements. The magnetoresistance contains a symmetric term independent of the cooling field and a linear term whose sign changes by inverting the polarity of a cooling field above ± 3 T. The Hall resistance also exhibits a non-zero value at 0 T which depends on lattice distortion due to epitaxial strain, leading to a scalar spin chirality that does not cancel out. Additionally, AHE with no net magnetization has also been reported in other works on $\text{Eu}_2\text{Ir}_2\text{O}_7$ films.¹⁷⁷

Fujita *et al.*¹⁸⁴ investigated the magnetic domain structure through the coupling between Tb^{3+} and Ir^{4+} moments in $\text{Tb}_2\text{Ir}_2\text{O}_7$ single-crystalline thin films, in which both sublattices form the AIAO magnetic structure at temperatures around 120 and 40 K, respectively, similar to the bulk material. Specifically, they studied how molecular fields of Tb^{3+} moments affect the magnetoresistance of Ir^{4+} below the ordering temperature of Tb^{3+} , which exhibits axial magnetocrystalline anisotropy along the [111] direction. The magnetic domain structure of the Ir^{4+} sublattice was controlled through the cooling procedure and analysed by the sign of the linear term of magnetoresistance.^{151,158} It was observed that Ir^{4+} moments experience opposite fields at temperatures lower or higher than the ordering temperature of Tb^{3+} . These results suggest that molecular fields from Tb^{3+} are antiparallel to the external field along the [111] direction. Additionally, in contrast to $\text{Nd}_2\text{Ir}_2\text{O}_7$, little contribution from domain-wall conduction was observed in $\text{Tb}_2\text{Ir}_2\text{O}_7$.

V. FUTURE RESEARCH DIRECTIONS

A. Chemical doping

Carrier doping has the potential to produce metals with emergent properties, enabling control of the band filling in the Ir 5d state through the chemical substitution of R^{3+} ions with divalent A ions, such as Ca, in doped pyrochlores (R_{1-x}A_x) $_2\text{Ir}_2\text{O}_7$. Intermediate band filling-controlled compounds exhibit novel phase transitions and related magneto-electronic phenomena,⁹⁴ although this has not been yet reported in thin films. Consequently, the effects of disorder introduced by doping on physical properties remain unexplored. Theoretical studies have also investigated possible phases on a pyrochlore lattice upon doping.²¹² Table II summarizes key experimental evidence found in polycrystalline hole-doped pyrochlore iridates, which can guide the exploration of epitaxial doped pyrochlore iridate films.

B. Design and growth of epitaxial heterostructures

Research on heterointerfaces between pyrochlore oxides holds significant potential for groundbreaking discoveries,^{213,214} much like those found at interfaces between the extensively investigated family of perovskite

oxides.^{11,12,15,215-219} But if studies on epitaxial films of pyrochlore oxides are at a very early stage, even more so on their interfaces, since additional challenges arise when integrating these films into heterostructures. Thus, experimental insight is currently lacking. b Theoretically, it was proposed that a metallic surface with topological nature and a ferromagnetic moment, distinct from the bulk antiferromagnetic insulator, will emerge at magnetic domain walls of $\text{R}_2\text{Ir}_2\text{O}_7$.²²⁰ This is triggered by the formation of Fermi arcs at the domain walls, which can be tuned through applied magnetic fields. These domain-wall states, induced by the chiral anomaly, enable Anderson localization by impurities. Under external magnetic fields they will show anomalous Hall conductivities.

This magnetic control of the interface electronic transport was studied experimentally in the epitaxial heterostructure $\text{Eu}_2\text{Ir}_2\text{O}_7/\text{Tb}_2\text{Ir}_2\text{O}_7$.¹⁵⁴ In this case, $\text{Eu}_2\text{Ir}_2\text{O}_7$ acts as the pinned layer and their magnetic domains AIAO or AOAI are determined by the cooling magnetic field, while those of $\text{Tb}_2\text{Ir}_2\text{O}_7$ are switched by a sweeping magnetic field. The authors reported the observation of additional conduction coming from the interface between domains of different type at both sides of the interface, that was not observed in single layers of neither of these pyrochlores.

This is the only heterostructure between epitaxial pyrochlore iridates experimentally studied so far.

From the theoretical side, formation of a two-dimensional magnetic monopole gas confined at the interface between a pyrochlore spin ice and an antiferromagnetic pyrochlore iridate has been suggested by means of Monte Carlo simulations with 2-in-2-out and all-in-all-out states at each side of the pyrochlore heterointerface.²²¹

Epitaxial heterostructures are promising platforms for investigating interactions between localized frustrated spins in quantum magnets, most of which are insulators, and conducting charge carriers. Therefore, these heterostructures can bridge the gap between fundamental research on insulating quantum magnets and potential electronic applications.

Recently, the interaction between localized moments and itinerant carriers at both sides of an epitaxial heterostructure has been studied as a means to achieve electrical detection of spin states in insulating quantum magnets. Zhang *et al.*²²² investigated an epitaxial pyrochlore structure in which ultra thin films of nonmagnetic metallic $\text{Bi}_2\text{Ir}_2\text{O}_7$ were grown on $\text{Dy}_2\text{Ti}_2\text{O}_7$ single crystals that exhibit spin ice behaviour. They observed anomalies in the magnetoresistance of $\text{Bi}_2\text{Ir}_2\text{O}_7$ when a magnetic field was applied along the [111] direction, at the same field intensity at which anomalies were observed in the AC susceptibility. These findings suggest that charge carriers from the metallic pyrochlore are sensitive to the spin flips of the spin ice pyrochlore, transitioning from the 2-in-2-out configuration to the 3-1/1-3 state.

Ohno *et al.*²²³ also explored the electrical detection of magnetic transitions in the spin ice insulator $\text{Dy}_2\text{Ti}_2\text{O}_7$ through its interface with a nonmagnetic pyrochlore metal. In this study, a relaxed $\text{Dy}_2\text{Ti}_2\text{O}_7$ film was grown on a $\text{La}_2\text{Zr}_2\text{O}_7$ buffer layer on a YSZ (111) substrate, ensuring no epitaxial strain occurs and allowing $\text{Dy}_2\text{Ti}_2\text{O}_7$ to exhibit magnetic properties similar to those of the bulk material. Subsequently, a film

TABLE II. Bulk polycrystalline hole-doped pyrochlore iridates

Material	Key experimental evidences
$(\text{Nd}_{1-x}\text{Pr}_x)_2\text{Ir}_2\text{O}_7$	Seebeck and Nernst signals are amplified for $x = 0.5$ in proximity to the field-induced metal-to-insulator transition. ²⁰⁵
$(\text{Eu}_{1-x}\text{Ca}_x)_2\text{Ir}_2\text{O}_7$, $(\text{Tb}_{1-x}\text{Ca}_x)_2\text{Ir}_2\text{O}_7$, $(\text{Gd}_{1-x}\text{Cd}_x)_2\text{Ir}_2\text{O}_7$	$(\text{Gd}_{1-x}\text{Cd}_x)_2\text{Ir}_2\text{O}_7$ and $(\text{Tb}_{1-x}\text{Ca}_x)_2\text{Ir}_2\text{O}_7$ exhibit a systematic reduction in resistivity and in the magnetic transition temperature as x increases and turn into a paramagnetic phase at sufficiently large x . For $x = 0.12$, $(\text{Gd}_{1-x}\text{Cd}_x)_2\text{Ir}_2\text{O}_7$ displays a large Hall effect driven by the magnetic exchange coupling between Gd $4f$ and Ir $5d$ moments. ⁹⁴
$(\text{Eu}_{1-x}\text{Ca}_x)_2\text{Ir}_2\text{O}_7$, $([\text{Nd}_{0.2}\text{Pr}_{0.8}]_{1-x}\text{Ca}_x)_2\text{Ir}_2\text{O}_7$, $(\text{Pr}_{1-x}\text{Ca}_x)_2\text{Ir}_2\text{O}_7$	Magnetization and magnetic transition temperature decrease with increasing x in $(\text{Eu}_{1-x}\text{Ca}_x)_2\text{Ir}_2\text{O}_7$, and the antiferromagnetic transition appears to vanish around $x = 0.05$. For $x \geq 0.05$, it shows metallic behaviour down to 2 K. The temperature dependence of the Seebeck coefficient shows a peak consistent with quadratic band touching point in a wide doping range in the doping-induced metallic phase. ⁹³
$(\text{Eu}_{1-x}\text{Ca}_x)_2\text{Ir}_2\text{O}_7$	MIT is fully suppressed within the doping range $0.04 < x < 0.07$, and the resistivity shows metallic behaviour for $x = 0.07$ and 0.13 , with no upturn observed down to 2 K. Short-range antiferromagnetic order (decoupled from the metal-to-insulator transition) persists into the metallic range. ²⁰⁶
$(\text{Eu}_{1-x}\text{Bi}_x)_2\text{Ir}_2\text{O}_7$	The ground state remains insulating for $x < 0.035$, while a metallic behaviour appears for $0.1 < x < 1$, with no signs of magnetic ordering. The temperature dependence resistivity changes from T linear ($x = 0.1$) to $T^{3/2}$ ($x \geq 0.5$) with a Fermi-liquid-like T^2 dependence at $x = 0.25$. ^{207,208}
$(\text{Nd}_{1-x}\text{Pr}_x)_2\text{Ir}_2\text{O}_7$, $(\text{Sm}_{1-x}\text{Nd}_x)_2\text{Ir}_2\text{O}_7$	Large magnetoresistance is observed for $(\text{Nd}_{1-x}\text{Pr}_x)_2\text{Ir}_2\text{O}_7$ with $0.4 < x < 0.7$ near the zero-field phase boundary between the antiferromagnetic insulator and the paramagnetic semimetal. The insulating phase below the transition temperature is systematically suppressed with increasing x , and a metallic state with no resistivity upturn down to 2 K and no magnetic order appears around $x = 0.8$. $(\text{Sm}_{1-x}\text{Nd}_x)_2\text{Ir}_2\text{O}_7$ exhibits a paramagnetic insulator-metal crossover for $y = 0.7 - 0.9$, reminiscent of a first-order Mott transition. ¹⁰⁴
$(\text{Nd}_{1-x}\text{Ca}_x)_2\text{Ir}_2\text{O}_7$	Suppression of MIT and AIAO order on the Ir sublattice with hole doping. For $0 < x < 0.08$, as doping level increases, the metal-to-insulator transition temperature decreases. For $x \geq 0.08$, the ground state becomes metallic with a weak upturn (likely due to disorder) in the low temperature range and signatures of Ir magnetic order vanish. ²⁰⁹
$(\text{Eu}_{1-x}\text{Sr}_x)_2\text{Ir}_2\text{O}_7$	Metal-insulator transition temperature reduced with hole doping. Non-Fermi liquid behaviour for $x = 0.2$. ²¹⁰
$(\text{Eu}_{1-x}\text{Nd}_x)_2\text{Ir}_2\text{O}_7$	Metal-insulator transition temperature decreases with increase in Nd content. Linear specific heat in the insulating region. ²¹¹

of $\text{Bi}_2\text{Rh}_2\text{O}_7$ (hosting a $4d$ metal at the B site instead of Ir) was epitaxially grown on $\text{Dy}_2\text{Ti}_2\text{O}_7$. A similar heterostructure could be made with a pyrochlore iridate, and this example is noteworthy as it demonstrates the functionalization of a pyrochlore quantum magnet through interface transport phenomena.

Specifically, changes of the spin structure in $\text{Dy}_2\text{Ti}_2\text{O}_7$ were controlled by a magnetic field along the $[111]$ direction, and its magnetic transitions were detected through the topological Hall effect in $\text{Bi}_2\text{Rh}_2\text{O}_7$, thanks to the proximity effect at the interface $\text{Bi}_2\text{Rh}_2\text{O}_7/\text{Dy}_2\text{Ti}_2\text{O}_7$. The noncoplanar spin configuration gives rise to an internal effective magnetic field, proportional to the spin chirality (solid angle subtended by the spins), whose sign changes when a magnetic field is applied along $[111]$, but not when the field is along the $[001]$ direction. Additionally, field-angle dependent longitudinal resistivity measured at a field of 9 T shows peaks that

can be attributed to the spin transitions in $\text{Dy}_2\text{Ti}_2\text{O}_7$ from the 2-in/2-out (2/2) to the 3-in/1-out (3/1) configuration (Fig.9), in contrast to the isotropic transport observed at the interface of $\text{Bi}_2\text{Rh}_2\text{O}_7$ with the nonmagnetic $\text{Eu}_2\text{Ti}_2\text{O}_7$. This study bridges fundamental research on insulating quantum magnets with potential electronic applications. The findings could lead to transformative innovations in quantum technologies by enabling electrical detection of emergent quantum phenomena.

C. Substrates for straining pyrochlore iridates

Epitaxial strain is a crucial parameter for inducing topological phenomena in pyrochlore iridates, as structural distortions lead to changes in the electronic structure due to electron-lattice coupling and break the cubic symmetry. Therefore, the growth of single-crystal pyrochlore substrates is an essential

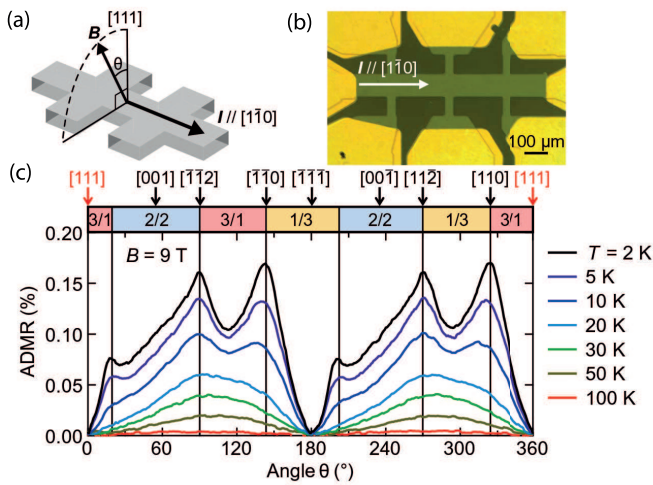


FIG. 9. Proximity effect at the epitaxial pyrochlore heterostructure $\text{Bi}_2\text{Rh}_2\text{O}_7/\text{Dy}_2\text{Ti}_2\text{O}_7$. (a) Measurement configuration of the field-angle dependent resistivity performed under a magnetic field. (b) Hall device structure used in the experiment. (c) Angle dependent magnetoresistance ($\text{ADMIR} = \rho_{xx}(\theta)/\rho_{xx}(0^\circ) - 1$) for several temperatures at 9 T. Crystallographic directions and expected magnetic structures of the Dy 4f moments are indicated in the upper part of the plot. M. Ohno *et al.*, *Science Advances*, 10(11), 10.1126/sciadv.adk6308, 2024; licensed under a Creative Commons Attribution (CC BY-NC) license.²²³

enabling technology for thin film investigations, facilitating the exploration of new phases.

Recently, pyrochlore substrates of $\text{Y}_2\text{Ti}_2\text{O}_7$ have become commercially available. Additionally, other pyrochlore oxides, such as $\text{Tb}_2\text{Ti}_2\text{O}_7$, $\text{Gd}_2\text{Ti}_2\text{O}_7$, $\text{Dy}_2\text{Ti}_2\text{O}_7$ and $\text{Ho}_2\text{Ti}_2\text{O}_7$,^{224–227} have been grown as bulk crystals using the Czochralski method. Thus, it is expected that single crystal substrates with pyrochlore structure will become more common in the near future, enabling growth thin films with tunable strain.

Alternatively, buffering a fluorite substrate with a pyrochlore oxide can also achieve different levels of structural distortions in the epitaxial films.²²⁸ Although this approach may compromise the functional of a heterostructure due to interfacial roughness, it has been validated as an effective method for providing an intermediate layer in the growth of a pyrochlore spin ice.²²³ In that case, the buffer layer was employed to obtain a pyrochlore spin ice film free from epitaxial strain with magnetic properties similar to those of bulk single crystals.

VI. CONCLUSIONS

Research on pyrochlore iridates can advance by building upon previous successful approaches that have been applied to simpler materials, such as studying novel phenomena at heterointerfaces. The outcomes of this research will indicate new research directions for functional materials, since interfacing oxides with pyrochlore structure remains an unexplored area.

Identifying combinations of materials with desired properties for specific applications will mark a breakthrough.

On the other hand, the technological relevance of pyrochlore oxides stems from the unusual types of fractionalized quasiparticles (emergent excitations of collective behaviour) that they can support, such as magnetic monopoles in pyrochlore titanates with a spin ice state or Weyl fermions in pyrochlore iridates with a magnetic Weyl semimetal state. These materials can potentially drive major technological innovations. It is hoped that this review will stimulate further discussions and research in this field.

AUTHOR DECLARATIONS

Conflict of Interest

The authors have no conflicts to disclose

DATA AVAILABILITY

Data sharing is not applicable to this article as no new data were created or analyzed in this study.

- ¹M. Imada, A. Fujimori, and Y. Tokura, *Reviews of Modern Physics* **70** (1998), 10.1103/RevModPhys.70.1039.
- ²Y. Tokura and N. Nagaosa, *Science* **288** (2000), 10.1126/science.288.5465.462.
- ³E. Dagotto, *Science* **309**, 257 (2005).
- ⁴A. Georges, L. de Medici, and J. Mravlje, *Annual Review of Condensed Matter Physics* **4**, 137 (2013).
- ⁵H. Ngai, F. Walker, and C. Ahn, *Annual Review of Materials Research* **44**, 1 (2014).
- ⁶A. Ohtomo and H. Y. Hwang, *Nature* **427**, 423 (2004).
- ⁷N. Reyren, S. Thiel, A. D. Caviglia, L. F. Kourkoutis, G. Hammerl, C. Richter, C. W. Schneider, T. Kopp, A.-S. Ruetschi, D. Jaccard, M. Gabay, D. A. Muller, J.-M. Triscone, and J. Mannhart, *Science* **317**, 1196 (2007).
- ⁸J. Mannhart, D. Blank, H. Hwang, A. Millis, and J.-M. Triscone, *MRS Bulletin* **33**, 1027 (2008).
- ⁹A. D. Caviglia, M. Gabay, S. Gariglio, N. Reyren, C. Cancellieri, and J.-M. Triscone, *Physical Review Letters* **104** (2010), 10.1103/PhysRevLett.104.126803.
- ¹⁰H. W. Jang, D. A. Felker, C. W. Bark, Y. Wang, M. K. Niranjan, C. T. Nelson, Y. Zhang, D. Su, C. M. Folkman, S. H. Baek, S. Lee, K. Janicka, Y. Zhu, X. Q. Pan, D. D. Fong, E. Y. Tsymlal, M. S. Rzchowski, and C. B. Eom, *Science* **331**, 886 (2011).
- ¹¹P. Zubko, S. Gariglio, M. Gabay, P. Ghosez, and J.-M. Triscone, *Annual Review of Condensed Matter Physics* **2** (2011), 10.1146/annurev-conmatphys-062910-140445.
- ¹²H. Y. Hwang, Y. Iwasa, M. Kawasaki, B. Keimer, N. Nagaosa, and Y. Tokura, *Nature Materials* **11** (2012), 10.1038/nmat3223.
- ¹³S. Stemmer and S. J. Allen, *Annual Review of Materials Research* **44** (2014), 10.1146/annurev-matsci-070813-113552.
- ¹⁴A. K. Yadav, C. T. Nelson, S. L. Hsu, Z. Hong, J. D. Clarkson, C. M. Schlepütz, A. R. Damodaran, P. Shafer, E. Arenholz, L. R. Dedon, D. Chen, A. Vishwanath, A. M. Minor, L. Q. Chen, J. F. Scott, L. W. Martin, and R. Ramesh, *Nature* **530** (2016), 10.1038/nature16463.
- ¹⁵Z. Huang, Ariando, X. R. Wang, A. Rusydi, J. Chen, H. Yang, and T. Venkatesan, *Advanced Materials* **30** (2018), 10.1002/adma.201802439.
- ¹⁶R. Ramesh and D. G. Schlom, *Nature Reviews Materials* **4** (2019), 10.1038/s41578-019-0095-2.
- ¹⁷K.-Y. Yang, Y.-M. Lu, and Y. Ran, *Physical Review B* **84** (2011), 10.1103/PhysRevB.84.075129.

- ¹⁸M. Coll, J. Fontcuberta, M. Althammer, M. Bibes, H. Boschker, A. Calleja, G. Cheng, M. Cuoco, R. Dittmann, B. Dkhil, I. E. Baggar, M. Fanciulli, I. Fina, E. Fortunato, C. Frontera, S. Fujita, V. Garcia, S. T. B. Goennenwein, C. G. Granqvist, J. Grollier, R. Gross, A. Hagfeldt, G. Herranz, K. Hono, E. Houwman, M. Huijben, A. Kalaboukhov, D. J. Keeble, G. Koster, L. F. Kourkoutis, J. Levy, M. Lira-Cantu, J. L. MacManus-Driscoll, J. Mannhart, R. Martins, S. Menzel, T. Mikołajick, M. Napoli, M. D. Nguyen, G. Niklasson, C. Paillard, S. Panigrahi, G. Rijnders, F. Sanchez, P. Sanchis, S. Sanna, D. G. Schlom, U. Schroeder, K. M. Shen, A. Siemon, M. Spreitzer, H. Sukegawa, R. Tamayo, J. van den Brink, N. Pryds, and F. M. Granozio, *Applied Surface Science* **482** (2019), 10.1016/j.apsusc.2019.03.312.
- ¹⁹C. A. F. Vaz, Y. J. Shin, M. Bibes, K. M. Rabe, F. J. Walker, and C. H. Ahn, *Applied Physics Review* **8** (2021), 10.1063/5.0060218.
- ²⁰T. J. Park, S. B. Deng, S. Manna, A. Islam, H. M. Yu, Y. F. Yuan, D. D. Fong, A. A. Chubykin, A. Sengupta, S. K. Sankaranarayanan, and S. Ramanathan, *Advanced Materials* **35** (2023), 10.1002/adma.202203352.
- ²¹J. B. Goodenough, *Reports on Progress in Physics* **67**, 1915 (2004).
- ²²B. Keimer and J. E. Moore, *Nature Physics* **13**, 1045 (2017).
- ²³Y. Tokura, M. Kawasaki, and N. Nagaosa, *Nature Physics* **13**, 1056 (2017).
- ²⁴N. Samarth, *Nature Materials* **16**, 1068 (2017).
- ²⁵D. N. Basov, R. D. Averitt, and D. Hsieh, *Nature Materials* **16**, 1077 (2017).
- ²⁶F. Giustino, J. H. Lee, F. Trier, M. Bibes, S. M. Winter, R. Valenti, Y. W. Son, L. Taillefer, C. Heil, A. I. Figueroa, B. Placais, Q. S. Wu, O. V. Yazyev, E. Bakkers, J. Nygard, P. Forn-Diaz, S. D. Franceschi, J. W. McIver, L. Torres, T. Low, A. Kumar, R. Galceran, S. O. Valenzuela, M. V. Costache, A. Manchon, E. A. Kim, G. R. Schleder, A. Fazzio, and S. Roche, *Journal of Physics-Materials* **3** (2020), 10.1088/2515-7639/abb74e.
- ²⁷C. Ahn, A. Cavalleri, A. Georges, S. Ismail-Beigi, A. J. Millis, and J.-M. Triscone, *Nature Materials* **20**, 1462 (2021).
- ²⁸J. A. Sobota, Y. He, and Z. X. Shen, *Review of Modern Physics* **93** (2021), 10.1103/RevModPhys.93.025006.
- ²⁹S. Paschen and Q. Si, *Nature Reviews Physics* **3** (2021), 10.1038/s42254-020-00262-6.
- ³⁰J. G. Checkelsky, B. A. Bernevig, P. Coleman, M. Si, and S. Paschen, *Nature Review Materials* (2024), 10.1038/s41578-023-00644-z.
- ³¹Q. Wang, H. Lei, Y. Qi, and C. Felser, *Accounts of Materials Research* **5**, 786 (2024).
- ³²M. Subramanian, G. Aravamudan, and G. V. S. Rao, *Prog. Solid State Chem.* **15**, 55 (1983).
- ³³J. S. Gardner, M. J. P. Gingras, and J. Greedan, *Reviews of Modern Physics* **82**, 53 (2010).
- ³⁴S. T. Bramwell and M. J. Harris, *Journal of Physics-Condensed Matter* **10**, L215 (1998).
- ³⁵S. T. Bramwell and M. J. P. Gingras, *Science* **294**, 1495 (2001).
- ³⁶J. E. Greedan, *Journal of Alloys and Compounds* **408**, 444 (2006).
- ³⁷M. N. Valdez and N. A. Spaldin, *Polyhedron* **171**, 181 (2019).
- ³⁸Y. Ishibashi and M. Iwata, *Journal of the Physical Society of Japan* **79** (2010), 10.1143/JPSJ.79.044604.
- ³⁹M. Hanawa, Y. Muraoka, T. Tayama, T. Sakakibara, J. Yamaura, and Z. Hiroi, *Physical Review Letters* **87** (2001), 10.1103/PhysRevLett.87.187001.
- ⁴⁰H. Sakai, K. Yoshimura, H. Ohno, H. Kato, S. Kambe, R. E. Walstedt, T. Matsuda, Y. Haga, and Y. Onuki, *Journal of Physics-Condensed Matter* **13**, L785 (2001).
- ⁴¹Z. Hiroi, J. I. Yamaura, T. C. Kobayashi, Y. Matsubayashi, and D. Hirai, *Journal of the Physical Society of Japan* **87** (2018), 10.7566/JPSJ.87.024702.
- ⁴²M. A. Subramanian, B. H. Toby, A. P. Ramirez, W. J. Marshall, A. W. Sleight, and G. H. Kwei, *Science* **273**, 81 (1996).
- ⁴³A. P. Ramirez and M. A. Subramanian, *Science* **277**, 546 (1997).
- ⁴⁴S. H. Oh, R. Black, E. Pomerantseva, J.-H. Lee, and L. F. Nazar, *Nature Chemistry* **4**, 1004 (2012).
- ⁴⁵J. Kim, P.-C. Shih, K.-C. Tsao, Y.-T. Pan, X. Yin, C.-J. Sun, and H. Yang, *Journal of the American Chemical Society* **139**, 12076 (2017).
- ⁴⁶D. Lebedev, M. Povia, K. Waltar, P. M. Abdala, I. E. Castelli, E. Fabbri, M. V. Blanco, A. Fedorov, C. Copéret, N. Marzari, and T. J. Schmidt, *Chemistry of Materials* **29**, 5182 (2017).
- ⁴⁷M. Kim, J. Park, M. Kang, J. Y. Kim, and S. W. Lee, *ACS Central Science* **6**, 880 (2020).
- ⁴⁸A. F. Fuentes, E. C. O'Quinn, S. M. Montemayor, H. Zhou, M. Lang, and R. C. Ewing, *Applied Physics Reviews* **11** (2024), 10.1063/5.0192415.
- ⁴⁹P. Gayen, S. Saha, and V. Ramani, *Accounts of Chemical Research* **55**, 2191 (2022).
- ⁵⁰S. Supriya, *Coordination Chemistry Reviews* **493** (2023), 10.1016/j.ccr.2023.215319.
- ⁵¹J. Lian, L. M. Wang, S. X. Wang, J. Chen, L. A. Boatner, and R. C. Ewing, *Physical Review Letters* **87** (2001), 10.1103/PhysRevLett.87.145901.
- ⁵²R. C. Ewing, W. J. Weber, and J. Lian, *Journal of Applied Physics* **95**, 5949 (2004).
- ⁵³K. E. Sickafus, L. Minervini, R. W. Grimes, J. A. Valdez, M. Ishimaru, F. Li, K. J. McClellan, and T. Hartmann, *Science* **289**, 748 (2000).
- ⁵⁴Y. Machida, S. Nakatsuji, Y. Maeno, T. Tayama, T. Sakakibara, and S. Onoda, *Physical Review Letters* **98** (2007), 10.1103/PhysRevLett.98.057203.
- ⁵⁵Y. Machida, S. Nakatsuji, S. Onoda, T. Tayama, and T. Sakakibara, *Nature Physics* **12**, 210 (2010).
- ⁵⁶K. Ueda, S. Iguchi, T. Suzuki, S. Ishiwata, Y. Taguchi, and Y. Tokura, *Physical Review Letters* **108** (2012), 10.1103/PhysRevLett.108.156601.
- ⁵⁷H. Fukuda, K. Ueda, Y. Kaneko, R. Kurihara, A. Miyake, K. Karube, M. Tokunaga, Y. Taguchi, and Y. Tokura, *Physical Review B* **106** (2022), 10.1103/PhysRevB.106.144431.
- ⁵⁸M. E. Brooks-Bartlett, S. T. Banks, L. D. C. Jaubert, A. Harman-Clarke, and P. C. W. Holdsworth, *Physical Review X* **4** (2014), 10.1103/PhysRevX.4.011007.
- ⁵⁹C. L. Henley, *Annual Review of Condensed Matter Physics* **1**, 179 (2010).
- ⁶⁰S. Petit, E. Lhotel, B. Canals, M. C. Hatnean, J. Ollivier, H. Mutka, E. Ressouche, A. R. Wildes, M. R. Lees, and G. Balakrishnan, *Nature Physics* **12**, 746 (2016).
- ⁶¹E. Lefrançois, V. Cathelin, E. Lhotel, J. Robert, P. Lejay, C. Colin, B. Canals, F. Damay, J. Ollivier, B. Fak, L. Chapon, R. Ballou, and V. Simonet, *Nature Communications* **8** (2017), 10.1038/s41467-017-00277-1.
- ⁶²E. Lhotel, L. D. C. Jaubert, and P. C. W. Holdsworth, *Journal of Low Temperature Physics* **201**, 710 (2020).
- ⁶³I. A. Ryzhkin, *Journal of Experimental and Theoretical Physics* **101**, 481 (2005).
- ⁶⁴C. Castelnovo, R. Moessner, and S. L. Sondhi, *Nature* **451**, 42 (2008).
- ⁶⁵S. T. Bramwell and M. J. Harris, *Journal of Physics-Condensed Matter* **32** (2020), 10.1088/1361-648X/ab8423.
- ⁶⁶T. Fennell, P. P. Deen, A. R. Wildes, K. Schmalzl, D. Prabhakaran, A. T. Boothroyd, R. J. Aldus, D. F. McMorrow, and S. T. Bramwell, *Science* **326**, 415 (2009).
- ⁶⁷S. T. Bramwell, S. R. Giblin, S. Calder, R. Aldus, D. Prabhakaran, and T. Fennell, *Nature* **461** (2009), 10.1038/nature08500.
- ⁶⁸L. D. C. Jaubert and P. C. W. Holdsworth, *Nature Physics* **5**, 258 (2009).
- ⁶⁹D. J. P. Morris, D. A. Tennant, S. A. Grigera, B. Klemke, C. Castelnovo, R. Moessner, C. Czternasty, M. Meissner, K. C. Rule, J.-U. Hoffmann, K. Kiefer, S. Gerischer, D. Slobinsky, and R. S. Perry, *Science* **326**, 411 (2009).
- ⁷⁰H. Kadowaki, N. Doi, Y. Aoki, Y. Tabata, T. J. Sato, J. W. Lynn, K. Matsuhira, and Z. Hiroi, *Journal of the Physical Society of Japan* **78** (2009), 10.1143/JPSJ.78.103706.
- ⁷¹A. Bansil, H. Lin, and T. Das, *Reviews of Modern Physics* **88** (2016), 10.1103/RevModPhys.88.021004.
- ⁷²P. Narang, C. A. C. Garcia, and C. Felser, *Nature Materials* **20**, 293 (2021).
- ⁷³J. Cayssol and J. N. Fuchs, *Journal of Physics-Materials* **4** (2021), 10.1088/2515-7639/abf0b5.
- ⁷⁴B. J. Wieder, B. Bradlyn, J. Cano, Z. Wang, M. G. Vergniory, L. Elcoro, A. A. Soluyanov, C. Felser, T. Neupert, N. Regnault, and B. A. Bernevig, *Nature Reviews Materials* **7** (2022), 10.1038/s41578-021-00380-2.
- ⁷⁵G. Jackeli and G. Khaliullin, *Physical Review Letters* **102** (2009), 10.1103/PhysRevLett.102.017205.
- ⁷⁶D. Pesin and L. Balents, *Nature Physics* **6** (2010), 10.1038/nphys1606.
- ⁷⁷W. Witczak-Krempa, G. Chen, Y. B. Kim, and L. Balents, *Annual Review of Condensed Matter Physics* **5**, 57 (2014).
- ⁷⁸R. Schaffer, E. K.-H. Lee, B.-J. Yang, and Y. B. Kim, *Reports on Progress in Physics* **79** (2016), 10.1088/0034-4885/79/9/094504.
- ⁷⁹W. Witczak-Krempa and Y. B. Kim, *Physical Review B* **85** (2012), 10.1103/PhysRevB.85.045124.

- ⁸⁰J. G. Rau, E. K.-H. Lee, and H.-Y. Kee, *Annual Review of Condensed Matter Physics* **7**, 195 (2016).
- ⁸¹G. Cao and P. Schlottmann, *Reports on Progress in Physics* **81** (2018), 10.1088/1361-6633/aaa979.
- ⁸²T. Takayama, J. Chaloupka, A. Smerald, G. Khaliullin, and H. Takagi, *Journal of the Physical Society of Japan* **90** (2021), 10.7566/jpsj.90.062001.
- ⁸³K. Matsuhira, M. Wakeshima, R. Nakanishi, T. Yamada, A. Nakamura, W. Kawano, S. Takagi, and Y. Hinatsu, *Journal of the Physical Society of Japan* **76** (2007), 10.1143/jpsj.76.043706.
- ⁸⁴B. J. Yang and Y. B. Kim, *Physical Review B* **82** (2010), 10.1103/PhysRevB.82.085111.
- ⁸⁵G. Chen and M. Hermele, *Physical Review B* **86** (2012), 10.1103/PhysRevB.86.235129.
- ⁸⁶L. Savary, E. G. Moon, and L. Balents, *Physical Review X* **4** (2014), 10.1103/PhysRevX.4.041027.
- ⁸⁷B. J. Yang and N. Nagaosa, *Physical Review Letters* **24** (2014), 10.1103/PhysRevLett.112.246402.
- ⁸⁸K. Ueda, J. Fujioka, and Y. Tokura, *Physical Review B* **93** (2016), 10.1103/PhysRevB.93.245120.
- ⁸⁹Y. Yamaji and M. Imada, *Physical Review B* **93** (2016), 10.1103/PhysRevB.93.195146.
- ⁹⁰P. Goswami, B. Roy, and S. D. Sarma, *Physical Review B* **95** (2017), 10.1103/PhysRevB.95.085120.
- ⁹¹K. Ueda, T. Oh, B.-J. Yang, R. Kaneko, J. Fujioka, N. Nagaosa, and Y. Tokura, *Nature Communications* **8** (2017), 10.1038/ncomms15515.
- ⁹²T. Oh, H. Ishizuka, and B. J. Yang, *Physical Review B* **96** (2018), 10.1103/PhysRevB.98.144409.
- ⁹³R. Kaneko, M.-T. Huebsch, S. Sakai, R. Arita, H. Shinaoka, K. Ueda, Y. Tokura, and J. Fujioka, *Physical Review B* **99** (2019), 10.1103/PhysRevB.99.161104.
- ⁹⁴K. Ueda, H. Fukuda, R. Kaneko, J. Fujioka, and Y. Tokura, *Physical Review B* **102** (2020), 10.1103/PhysRevB.102.245131.
- ⁹⁵M. C. Shapiro, S. C. Riggs, M. B. Stone, C. R. de la Cruz, S. Chi, A. A. Podlesnyak, and I. R. Fisher, *Physical Review B* **85** (2012), 10.1103/PhysRevB.85.214434.
- ⁹⁶J. P. Clancy, H. Gretarsson, E. K. H. Lee, D. Tian, J. Kim, M. H. Upton, D. Casa, T. Gog, Z. Islam, B. G. Jeon, K. H. Kim, S. Desgreniers, Y. B. Kim, S. J. Julian, and Y. J. Kim, *Physical Review B* **94** (2016), 10.1103/PhysRevB.94.024408.
- ⁹⁷H. Takatsu, K. Watanabe, K. Goto, and H. Kadowaki, *Physical Review B* **90** (2014), 10.1103/PhysRevB.90.235110.
- ⁹⁸X. Wan, A. M. Turner, A. Vishwanath, and S. Y. Savrasov, *Physical Review B* **83** (2011), 10.1103/PhysRevB.83.205101.
- ⁹⁹N. Nagaosa, T. Morimoto, and Y. Tokura, *Nature Reviews Materials* **5**, 621 (2020).
- ¹⁰⁰B. Q. Lv, T. Qian, and H. Ding, *Reviews of Modern Physics* **93** (2021), 10.1103/RevModPhys.93.025002.
- ¹⁰¹K. Ueda, R. Kaneko, H. Ishizuka, J. Fujioka, N. Nagaosa, and Y. Tokura, *Nature Communications* **9** (2018), 10.1038/s41467-018-05530-9.
- ¹⁰²K. Ueda, J. Fujioka, Y. Takahashi, T. Suzuki, S. Ishiwata, Y. Taguchi, M. Kawasaki, and Y. Tokura, *Physical Review B* **89** (2014), 10.1103/PhysRevB.89.075127.
- ¹⁰³E. Y. Ma, Y.-T. Cui, K. Ueda, S. Tang, K. Chen, N. Tamura, P. M. Wu, J. Fujioka, Y. Tokura, and Z.-X. Shen, *Science* **350**, 538 (2015).
- ¹⁰⁴K. Ueda, J. Fujioka, C. Terakura, and Y. Tokura, *Physical Review B* **92** (2015), 10.1103/PhysRevB.92.121110.
- ¹⁰⁵Z. Tian, Y. Kohama, T. Tomita, H. Ishizuka, T. H. Hsieh, J. J. Ishikawa, K. Kindo, L. Balents, and S. Nakatsuji, *Nature Physics* **12** (2016), 10.1038/nphys3567.
- ¹⁰⁶L. Hozoi, H. Gretarsson, J. P. Clancy, B.-G. Jeon, B. Lee, K. H. Kim, V. Yushankhai, P. Fulde, D. Casa, T. Gog, J. Kim, A. H. Said, M. H. Upton, Y.-J. Kim, and J. van den Brink, *Physical Review B* **89** (2014), 10.1103/PhysRevB.89.115111.
- ¹⁰⁷D. G. Schlom, L.-Q. Chen, X. Pan, A. Schmehl, and M. A. Zurbuchen, *Journal of the American Ceramic Society* **91**, 2429 (2008).
- ¹⁰⁸P. G. Evans, Y. Chen, J. A. Tilka, S. E. Babcock, and T. F. Kuech, *Current Opinion in Solid State & Materials Science* **22**, 229 (2018).
- ¹⁰⁹W. J. Kim, J. Song, Y. Li, and T. W. Noh, *APL Materials* **10** (2022), 10.1063/5.0097608.
- ¹¹⁰F. V. E. Hensling, W. Braun, D. Y. Kim, L. N. Majer, S. Smink, B. D. Faeth, and J. Mannhart, *APL Materials* **12** (2024), 10.1063/5.0196883.
- ¹¹¹C. B. Alcock and G. W. Hooper, *Proceedings of the Royal Society of London Series A-Mathematical and Physics Sciences* **254** (1960), 10.1098/rspa.1960.0040.
- ¹¹²S. Nair, Z. Yang, D. Lee, S. Guo, J. T. Sadowski, S. Johnson, A. Saboor, Y. Li, H. Zhou, R. B. Comes, W. Jin, K. A. Mkhoyan, A. Janotti, and B. Jalan, *Nat. Nanotechnol.* **18** (2023), 10.1038/s41565-023-01397-0.
- ¹¹³L. Savary and L. Balents, *Physical Review Letters* **118** (2017), 10.1103/PhysRevLett.118.087203.
- ¹¹⁴T. Taniguchi, H. Kadowaki, H. Takatsu, B. Fak, J. Ollivier, T. Yamazaki, T. J. Sato, H. Yoshizawa, Y. Shimura, T. Sakakibara, T. Hong, K. Goto, L. R. Yaraskavitch, and J. B. Kycia, *Physical Review B* **87** (2013), 10.1103/PhysRevB.87.060408.
- ¹¹⁵L. D. C. Jaubert, O. Benton, J. G. Rau, J. Oitmaa, R. R. P. Singh, N. Shannon, and M. J. P. Gingras, *Physics Review Letters* **115** (2015), 10.1103/PhysRevLett.115.267208.
- ¹¹⁶D. Bowman, E. Cemal, T. Lehner, A. Wildes, L. Mangin-Thro, G. Nilsen, M. Gutmann, D. Voneshen, D. Prabhakaran, A. Boothroyd, D. Porter, C. Castelnovo, K. Refson, and J. Goff, *Nature Communications* **10** (2019), 10.1038/s41467-019-08598-z.
- ¹¹⁷J. H. Haeni, P. Irvin, W. Chang, R. Uecker, P. Reiche, Y. L. Li, S. Choudhury, W. Tian, M. E. Hawley, B. Craigo, A. K. Tagantsev, X. Q. Pan, S. K. Streiffer, L. Q. Chen, S. W. Kirchoefer, J. Levy, and D. G. Schlom, *Nature* **430**, 758 (2004).
- ¹¹⁸J. H. Lee, L. Fang, E. Vlahos, X. Ke, Y. W. Jung, L. F. Kourkoutis, J.-W. Kim, P. J. Ryan, T. Heeg, M. Roeckerath, V. Goian, M. Bernhagen, R. Uecker, P. C. Hammel, K. M. Rabe, S. Kamba, J. Schubert, J. W. Freeland, D. A. Muller, C. J. Fennie, P. Schiffer, V. Gopalan, E. Johnston-Halperin, and D. G. Schlom, *Nature* **466** (2010), 10.1038/nature09331.
- ¹¹⁹D. G. Schlom, L.-Q. Chen, C. J. Fennie, V. Gopalan, D. A. Muller, X. Pan, R. Ramesh, and R. Uecker, *MRS Bulletin* **39**, 118 (2014).
- ¹²⁰R. Uecker, R. Bertram, M. Brutzam, Z. Galazka, T. M. Gering, C. Gugschev, D. Klimm, M. Klupsch, A. Kwasniewski, and D. G. Schlom, *Journal of Crystal Growth* **457**, 137 (2017).
- ¹²¹D. Sando, *Journal of Physics-Condensed Matter* **34** (2022), 10.1088/1361-648X/ac4c61.
- ¹²²T. Y. Li, S. Q. Deng, H. Liu, and J. Chen, *Chemical Reviews* **124**, 7045 (2024).
- ¹²³T. Ohtsuki, Z. Tian, A. Endo, M. Halim, S. Katsumoto, Y. Kohama, K. Kindo, M. Lippmaa, and S. Nakatsuji, *Proceedings of the National Academy of Sciences of the United States of America* **116** (2019), 10.1073/pnas.1819489116.
- ¹²⁴L. Guo, N. Campbell, Y. Choi, J.-W. Kim, P. J. Ryan, H. Huyan, L. Li, T. Nan, J.-H. Kang, C. Sundahl, X. Pan, M. S. Rzechowski, and C.-B. Eom, *Physical Review B* **101** (2020), 10.1103/PhysRevB.101.104405.
- ¹²⁵W. J. Kim, T. Oh, J. Song, E. K. Ko, Y. Li, J. Mun, B. Kim, J. Son, Z. Yang, Y. Kohama, M. Kim, B.-J. Yang, and T. W. Noh, *Science Advances* **6** (2020), 10.1126/sciadv.abb1539.
- ¹²⁶J. Chakhalian, X. Liu, and G. A. Fiete, *APL Materials* **8** (2020), 10.1063/5.0009092.
- ¹²⁷L. Minervini, R. W. Grimes, Y. Tabira, R. L. Withers, and K. E. Sickafus, *Philosophical Magazine A-Physics of Condensed Matter Structure Defects and Mechanical Properties* **82**, 123 (2002).
- ¹²⁸X. Hu, A. Ruedg, and G. A. Fiete, *Physical Review B* **86** (2012), 10.1103/PhysRevB.86.235141.
- ¹²⁹Q. Chen, H.-H. Hung, X. Hu, and G. A. Fiete, *Physical Review B* **92** (2015), 10.1103/PhysRevB.92.085145.
- ¹³⁰L. Minervini and R. W. Grimes, *Journal of the American Ceramic Society* **83**, 1873 (2000).
- ¹³¹M. V. Talanov and V. M. Talanov, *Chemistry of Materials* **33**, 2706 (2021).
- ¹³²S. Koohpayeh, J.-J. Wena, B. Trumpa, C. Broholm, and T. McQueen, *Journal of Crystal Growth* **402**, 291 (2014).
- ¹³³B. Trump, S. Koohpayeh, K. Livi, J.-J. Wen, K. Arpino, Q. Ramasse, R. Brydson, M. Feyngenson, H. Takeda, M. Takigawa, K. Kimura, S. Nakatsuji, C. Broholm, and T. McQueen, *Nature Communications* **9** (2018), 10.1038/s41467-018-05033-7.
- ¹³⁴C. H. Booth, J. S. Gardner, G. H. Kwei, R. H. Heffner, F. Bridges, and M. A. Subramanian, *Physical Review B* **62** (2000), 10.1103/PhysRevB.62.R755.

- ¹³⁵A. Andreanov, J. T. Chalker, T. E. Saunders, and D. Sherrington, *Phys. Rev. B* **81** (2010), 10.1103/PhysRevB.81.014406.
- ¹³⁶J.-J. Wen, S. M. Koohpayeh, K. A. Ross, B. A. Trump, T. M. McQueen, K. Kimura, S. Nakatsuji, Y. Qiu, D. M. Pajerowski, J. R. D. Copley, and C. L. Broholm, *Physical Review Letters* **118** (2017), 10.1103/PhysRevLett.118.107206.
- ¹³⁷N. Martin, P. Bonville, E. Lhotel, S. Guitteny, A. Wildes, C. Decorse, M. C. Hatnean, G. Balakrishnan, I. Mirebeau, and S. Petit, *Physical Review X* **7** (2017), 10.1103/PhysRevX.7.041028.
- ¹³⁸O. Benton, *Physical Review Letters* **121** (2018), 10.1103/PhysRevLett.121.037203.
- ¹³⁹E. C. O'Quinn, K. E. Sickafus, R. C. Ewing, G. Baldinozzi, J. C. Neufeind, M. G. Tucker, A. F. Fuentes, D. Drey, and M. K. Lang, *Science Advances* **6** (2020), 10.1126/sciadv.abc2758.
- ¹⁴⁰S. Nakatsuji, Y. Machida, Y. Maeno, T. Tayama, T. Sakakibara, J. van Duijn, L. Balicas, J. N. Millican, R. T. Macaluso, and J. Y. Chan, *Physical Review Letters* **96** (2006), 10.1103/PhysRevLett.96.087204.
- ¹⁴¹Y. Tokiwa, J. J. Ishikawa, S. Nakatsuji, and P. Gegenwart, *Natura Materials* **13**, 356 (2014).
- ¹⁴²Y. Taguchi, Y. Oohara, H. Yoshizawa, N. Nagaosa, and Y. Tokura, *Science* **291** (2001), 10.1126/science.1058161.
- ¹⁴³A. Go, W. Witzczak-Krempa, G. S. Jeon, K. Park, and Y. B. Kim, *Physical Review Letters* **109** (2012), 10.1103/PhysRevLett.109.066401.
- ¹⁴⁴W. Witzczak-Krempa, A. Go, and Y. B. Kim, *Physical Review B* **87** (2013), 10.1103/PhysRevB.87.155101.
- ¹⁴⁵M. Imada, Y. Yamaji, and M. Kurita, *Journal of the Physical Society of Japan* **83** (2014), 10.7566/jpsj.83.061017.
- ¹⁴⁶K. Ladovrechis, T. Meng, and B. Roy, *Physical Review B* **103** (2021), 10.1103/PhysRevB.103.L241116.
- ¹⁴⁷H. Guo, C. Ritter, and A. C. Komarek, *Physical Review B* **94** (2016), 10.1103/PhysRevB.94.161102.
- ¹⁴⁸R. Asih, N. Adam, S. S. Mohd-Tajudin, D. P. Sari, K. Matsuhira, H. Guo, M. Wakeshima, Y. Hinatsu, T. Nakano, Y. Nozue, S. Sulaiman, M. I. Mohamed-Ibrahim, P. K. Biswas, and I. Watanabe, *Journal of the Physical Society of Japan* **86** (2017), 10.7566/jpsj.86.024705.
- ¹⁴⁹K. Ueda, J. Fujioka, B.-J. Yang, J. Shioyai, A. Tsukazaki, S. Nakamura, S. Awaji, N. Nagaosa, and Y. Tokura, *Physical Review Letters* **115** (2015), 10.1103/PhysRevLett.115.056402.
- ¹⁵⁰H. Sagayama, D. Uematsu, T. Arima, K. Sugimoto, J. J. Ishikawa, E. O'Farrell, and S. Nakatsuji, *Physical Review B* **87** (2013), 10.1103/PhysRevB.87.100403.
- ¹⁵¹T. C. Fujita, Y. Kozuka, M. Uchida, A. Tsukazaki, T. Arima, and M. Kawasaki, *Scientific Reports* **5** (2015), 10.1038/srep09711.
- ¹⁵²T. C. Fujita, M. Uchida, Y. Kozuka, S. Ogawa, A. Tsukazaki, T. Arima, and M. Kawasaki, *Applied Physics Letters* **108** (2016), 10.1063/1.4939742.
- ¹⁵³E. Lefrançois, V. Simonet, R. Ballou, E. Lhotel, A. Hadj-Azzem, S. Kodjikian, P. Lejay, P. Manuel, D. Khalyavin, and L. C. Chapon, *Physical Review Letters* **114** (2015), 10.1103/PhysRevLett.114.247202.
- ¹⁵⁴T. C. Fujita, M. Uchida, Y. Kozuka, W. Sano, A. Tsukazaki, T. Arima, and M. Kawasaki, *Physical Review B* **93** (2016), 10.1103/PhysRevB.93.064419.
- ¹⁵⁵C. Donnerer, M. C. Rahn, E. Schierle, R. S. Perry, L. S. I. Veiga, G. Nisbet, S. P. Collins, D. Prabhakaran, A. T. Boothroyd, and D. F. McMorrow, *Journal of Physics-Condensed Matter* **34** (31), 10.1088/1361-648X/ab2217.
- ¹⁵⁶C. Donnerer, M. C. Rahn, M. M. Sala, J. G. Vale, D. Pincini, J. Strempler, M. Krisch, D. Prabhakaran, A. T. Boothroyd, and D. F. McMorrow, *Physical Review Letters* **117** (2016), 10.1103/PhysRevLett.117.037201.
- ¹⁵⁷H. Jacobsen, C. D. Dashwood, E. Lhotel, D. Khalyavin, P. Manuel, R. Stewart, D. Prabhakaran, D. F. McMorrow, and A. T. Boothroyd, *Physical Review B* **101** (2020), 10.1103/PhysRevB.101.104404.
- ¹⁵⁸T. Arima, *Journal of the Physical Society of Japan* **82** (2013), 10.7566/jpsj.82.013705.
- ¹⁵⁹K. Tomiyasu, K. Matsuhira, K. Iwasa, M. Watahiki, S. Takagi, M. Wakeshima, Y. Hinatsu, M. Yokoyama, K. Ohoyama, and K. Yamada, *Journal of the Physical Society of Japan* **81** (2012), 10.1143/jpsj.81.034709.
- ¹⁶⁰E. Lefrançois, L. Mangin-Thro, E. Lhotel, J. Robert, S. Petit, V. Cathelin, H. E. Fischer, C. V. Colin, F. Damay, J. Ollivier, P. Lejay, L. C. Chapon, V. Simonet, and R. Ballou, *Physical Review B* **99** (2019), 10.1103/PhysRevB.99.060401.
- ¹⁶¹M. J. Pearce, K. Gotze, A. Szabo, T. S. Sikken, M. R. Lees, A. T. Boothroyd, D. Prabhakaran, C. Castellano, and P. A. Goddard, *Nature Communications* **13** (2022), 10.1038/s41467-022-27964-y.
- ¹⁶²V. Cathelin, E. Lefrançois, J. Robert, P. C. Guruciaga, C. Paulsen, D. Prabhakaran, P. Lejay, F. Damay, J. Ollivier, B. Fak, L. C. Chapon, R. Ballou, V. Simonet, P. C. W. Holdsworth, and E. Lhotel, *Physical Review Research* **2** (2020), 10.1103/PhysRevResearch.2.032073.
- ¹⁶³O. Tchernyshyov and G. W. Chern, "Introduction to frustrated magnetism: materials, experiments, theory," (Springer, 2011) Chap. Spin-lattice coupling in frustrated antiferromagnets.
- ¹⁶⁴C. Castellano, G. Berti, S. Sanna, R. Ruiz-Bustos, J. van Duijn, A. Brambilla, A. Munoz-Noval, P. Carretta, L. Duo, and F. Demartin, *Physical Review B* **91** (2015), 10.1103/PhysRevB.91.224101.
- ¹⁶⁵T. T. A. Lommen, I. P. Handayani, M. C. Donker, D. Fausti, G. Dhallenne, P. Berthet, A. Revcolevschi, and P. H. M. van Loosdrecht, *Physical Review B* **77** (2008), 10.1103/PhysRevB.77.214310.
- ¹⁶⁶J. Son, B. C. Park, C. H. Kim, H. Cho, S. Y. Kim, L. J. Sandilands, C. Sohn, J. G. Park, S. J. Moon, and T. W. Noh, *npj Quantum Materials* **4** (2019), 10.1038/s41535-019-0157-0.
- ¹⁶⁷K. Ueda, R. Kaneko, A. Subedi, M. Minola, B. J. Kim, J. Fujioka, Y. Tokura, and B. Keimer, *Physical Review B* **100** (2019), 10.1103/PhysRevB.100.115157.
- ¹⁶⁸T. Uehara, T. Ohtsuki, M. Udagawa, S. Nakatsuji, and Y. Machida, *Nature Communications* **13** (2022), 10.1038/s41467-022-32375-0.
- ¹⁶⁹T. Ohtsuki, Z. Tian, M. Halim, S. Nakatsuji, and M. Lippmaa, *Journal of Applied Physics* **127** (2020), 10.1063/1.5128537.
- ¹⁷⁰Y. Li, T. Oh, J. Son, J. Song, M. K. Kim, D. Song, S. Kim, S. H. Chang, C. Kim, B. J. Yang, and T. W. Noh, *Advanced Materials* **33** (2021), 10.1002/adma.202008528.
- ¹⁷¹L. Guo, S.-L. Shang, N. Campbell, P. G. Evans, M. Rzczowski, Z.-K. Liu, and C.-B. Eom, *Npj Computational Materials* **7** (2021), 10.1038/s41524-021-00610-9.
- ¹⁷²J. C. Gallagher, B. D. Esser, R. Morrow, S. R. Dunsiger, R. E. A. Williams, P. M. Woodward, D. W. McComb, and F. Y. Yang, *Scientific Reports* **6** (2016), 10.1038/srep22282.
- ¹⁷³W. J. Kim, J. H. Gruenewald, T. Oh, S. Cheon, B. Kim, O. B. Korneta, H. Cho, D. Lee, Y. Kim, M. Kim, J.-G. Park, B.-J. Yang, A. Seo, and T. W. Noh, *Physical Review B* **98** (2018), 10.1103/PhysRevB.98.125103.
- ¹⁷⁴J. Song, E. K. Ko, S. Lee, J. Mun, J. H. Jeong, J. H. Lee, W. J. Kim, M. Kim, Y. Li, J. H. Lee, and T. W. Noh, *APL Materials* **11** (2023), 10.1063/5.0153164.
- ¹⁷⁵S. C. Shen, T. Oh, J. Song, D. Tian, X. Y. Shu, Y. Zhang, F. Zhang, D. Yi, T. W. Noh, B. J. Yang, Y. Y. Li, and P. Yu, *Advanced Materials* (2024), 10.1002/adma.202403306.
- ¹⁷⁶M. Ghosh, P. D. Babu, and P. S. A. Kumar, *APL Materials* **11** (2023), 10.1063/5.0166455.
- ¹⁷⁷X. Liu, S. Fang, Y. Fu, W. Ge, M. Kareev, J.-W. Kim, Y. Choi, E. Karapetrova, Q. H. Zhang, L. Gu, E. S. Choi, F. D. Wen, J. H. Wilson, G. Fabbri, P. J. Ryan, J. W. Freeland, D. Haskel, W. Wu, J. H. Pixley, and J. Chakhalian, *Physical Review Letters* **127** (2021), 10.1103/PhysRevLett.127.277204.
- ¹⁷⁸X. Liu, F. Wen, E. Karapetrova, J.-W. Kim, P. J. Ryan, J. W. Freeland, M. Terilli, T.-C. Wu, M. Kareev, and J. Chakhalian, *Applied Physics Letters* **117** (2020), 10.1063/5.0019876.
- ¹⁷⁹M. Ghosh, S. G. Bhat, A. Pal, and P. S. A. Kumar, *Journal of Physics-Condensed Matter* **34** (2022), 10.1088/1361-648X/ac50da.
- ¹⁸⁰M. Ghosh, D. Samal, and P. S. A. Kumar, *Physical Review B* **106** (2022), 10.1103/PhysRevB.106.085139.
- ¹⁸¹M. Ghosh, D. Samal, and P. S. A. Kumar, *Applied Physics Letters* **123** (2023), 10.1063/5.0172127.
- ¹⁸²X. Wu, Z. Wang, Z. Ding, Z. Lin, M. Yang, M. Gu, M. Meng, F. Yang, X. Liu, and J. Guo, *Applied Physics Letters* **124** (2024), 10.1063/5.0189226.
- ¹⁸³Y. Kozuka, T. C. Fujita, M. Uchida, T. Nojima, A. Tsukazaki, J. Matsuno, T. Arima, and M. Kawasaki, *Physical Review B* **96** (2017), 10.1103/PhysRevB.96.224417.
- ¹⁸⁴T. C. Fujita, Y. Kozuka, J. Matsuno, M. Uchida, A. Tsukazaki, T. Arima, and M. Kawasaki, *Physical Review Materials* **2** (2018), 10.1103/PhysRev-

- Materials.2.011402.
- ¹⁸⁵D. Oka and T. Fukumura, *Crystengcomm* **19**, 2144 (2017).
- ¹⁸⁶L. W. Martin, Y. H. Chu, and R. Ramesh, *Materials Science and Engineering R-Reports* **68**, III (2010).
- ¹⁸⁷S. A. Chambers, *Advanced Materials* **22**, 219 (2010).
- ¹⁸⁸D. H. Lowndes, D. B. Geohegan, A. A. Poretzky, D. P. Norton, and C. M. Rouleau, *Science* **273**, 898 (1996).
- ¹⁸⁹H. M. Christen and G. Eres, *Journal of Physics-Condensed Matter* **20** (2008), 10.1088/0953-8984/20/26/264005.
- ¹⁹⁰R. Groenen, J. Smit, K. Orsel, A. Vailionis, B. Bastiaens, M. Huijben, K. Bollner, G. Rijnders, and G. Koster, *APL Materials* **3** (2015), 10.1063/1.4926933.
- ¹⁹¹A. Brewer, K. H. Cho, W. Saenrang, S. H. Baek, J. C. Frederick, and C. B. Eom, *Journal of Vacuum Science Technology A* **35** (2017), 10.1116/1.4998956.
- ¹⁹²D. G. Schlom, *APL Materials* **3** (2015), 10.1063/1.4919763.
- ¹⁹³M. Brahlek, A. S. Gupta, J. Lapano, J. Roth, H.-T. Zhang, L. Zhang, R. Haislmaier, and R. Engel-Herbert, *Advanced Functional Materials* **28** (2018), 10.1002/adfm.201702772.
- ¹⁹⁴G. Rimal and R. B. Comes, *J. Phys. D-Appl. Phys.* **57** (2024), 10.1088/1361-6463/ad2569.
- ¹⁹⁵E. H. P. Cordfunke and G. Meyer, *Recueil des Travaux Chimiques des Pays-Bas-Journal of the Royal Netherlands Chemical Society* **81** (1962), 10.1002/recl.19620810608.
- ¹⁹⁶R. T. Wimber and H. G. Kraus, *Metallurgical Transactions* **5**, 1565 (1974).
- ¹⁹⁷J. K. Kawasaki, M. Uchida, H. Paik, D. G. Schlom, and K. M. Shen, *Physical Review B* **94** (2016), 10.1103/PhysRevB.94.121104.
- ¹⁹⁸M. A. Anderson, I. E. Baggari, C. M. Brooks, T. Powell, C. Lygouras, A. T. N'Diaye, S. M. Koohpayeh, J. Nordlander, and J. A. Mundy, *Chemistry of Materials* **33**, 2325 (2024).
- ¹⁹⁹W. J. Kim, E. K. Ko, S. Y. Kim, B. Kim, and T. W. Noh, *Current Applied Physics* **19**, 400 (2019).
- ²⁰⁰O. Hellman, *Materials Science and Engineering R-Reports* **16** (1996), 10.1016/0927-796X(96)80001-5.
- ²⁰¹D. E. MacLaughlin, O. O. Bernal, L. Shu, J. Ishikawa, Y. Matsumoto, J.-J. Wen, M. Mourigal, C. Stock, G. Ehlers, C. L. Broholm, Y. Machida, K. Kimura, S. Nakatsuji, Y. Shimura, and T. Sakakibara, *Physical Review B* **92** (2015), 10.1103/PhysRevB.92.054432.
- ²⁰²P. Telang, K. Mishra, A. K. Sood, and S. Singh, *Physical Review B* **97** (2018), 10.1103/PhysRevB.97.235118.
- ²⁰³K. Ueda, H. I. M. Kriener, S. Kitou, D. Maryenko, M. Kawamura, T. h Arima, M. Kawasaki, and Y. Tokura, *Physical Review B* **105** (2022), 10.1103/PhysRevB.105.L161102.
- ²⁰⁴M. T. Suzuki, M. Koretsune, M. Ochi, and R. Arita, *Physical Review B* **95** (2017), 10.1103/PhysRevB.95.094406.
- ²⁰⁵K. Ueda, J. Fujioka, N. Kanazawa, and Y. Tokura, *APL Materials* **10** (2022), 10.1063/5.0097460.
- ²⁰⁶E. Zoghlin, Z. Porter, S. Britner, S. Husremovic, Y. Choi, D. Haskel, G. Laurita, and S. D. Wilson, *Journal of Physics-Condensed Matter* **33** (2021), 10.1088/1361-648X/abbf2b.
- ²⁰⁷P. Telang, K. Mishra, G. Prando, A. K. Sood, and S. Singh, *Physical Review B* **99** (2019), 10.1103/PhysRevB.99.201112.
- ²⁰⁸P. Telang, A. Bandyopadhyay, K. Mishra, D. Rout, R. Bag, A. Gloskovskii, Y. Matveyev, and S. Singh, *Journal of Physics-Condensed Matter* **34** (2022), 10.1088/1361-648X/ac8038.
- ²⁰⁹Z. Porter, E. Zoghlin, S. Britner, S. Husremovic, J. P. C. Ruff, Y. Choi, D. Haskel, G. Laurita, and S. D. Wilson, *Physical Review B* **100** (2019), 10.1103/PhysRevB.100.054409.
- ²¹⁰A. Banerjee, J. Sannigrahi, S. Giri, and S. Majumdar, *Physical Review B* **96** (2017), 10.1103/PhysRevB.96.224426.
- ²¹¹S. Mondal, M. Modak, B. Maji, M. K. Ray, S. Mandal, S. K. Mandal, M. Sardar, and S. Banerjee, *Physical Review B* **102** (2020), 10.1103/PhysRevB.102.155139.
- ²¹²C. Berke, P. Michetti, and C. Timm, *New Journal of Physics* **20** (2018), 10.1088/1367-2630/aab881.
- ²¹³M. Uchida and M. Kawasaki, *Journal of Physics D-Applied Physics* **51** (2018), 10.1088/1361-6463/aaaf00.
- ²¹⁴H. Boschker and J. Mannhart, *Annual Review of Condensed Matter Physics* **8**, 145 (2017).
- ²¹⁵J. Chakhalian, J. W. Freeland, A. J. Millis, C. Panagopoulos, and J. M. Rondinelli, *Review of Modern Physics* **86** (2014), 10.1103/RevModPhys.86.1189.
- ²¹⁶J. A. Sulpizio, S. Ilani, P. Irvin, and J. Levy, *Annual Review of Materials Research* **44** (2014), 10.1146/annurev-matsci-070813-113437.
- ²¹⁷F. Hellman, A. Hoffmann, Y. Tserkovnyak, G. Beach, E. E. Fullerton, C. Leighton, A. H. MacDonald, D. Ralph, D. A. Arena, H. A. Dürr, P. Fischer, J. Grollier, J. P. Heremans, T. Jungwirth, A. V. Kimel, B. Koopmans, I. N. Krivorotov, S. J. May, A. K. Petford-Long, J. M. Rondinelli, N. Samarth, I. K. Schuller, A. N. Slavin, M. D. Stiles, O. T. A. Thiaville, and B. L. Zink, *Reviews of Modern Physics* **89** (2017), 10.1103/RevModPhys.89.025006.
- ²¹⁸A. Bhattacharya and S. J. May, *Annual Review of Materials Research* **44**, 65 (2014).
- ²¹⁹S. G. Jeong, J. Y. Oh, L. Hao, J. Liu, and W. S. Choi, *Advanced Functional Materials* **33** (2023), 10.1002/adfm.202301770.
- ²²⁰Y. Yamaji and M. Imada, *Physical Review X* **4** (2014), 10.1103/PhysRevX.4.021035.
- ²²¹L. Miao, Y. Lee, A. Mei, M. Lawler, and K. Shen, *Nature Communications* **11** (2020), 10.1038/s41467-020-15213-z.
- ²²²H. Zhang, C. Xing, K. Noordhoek, Z. Liu, T. Zhao, L. Horak, Q. Huang, L. Hao, J. Yang, S. Pandey, E. Dagotto, Z. G. Jiang, J. H. Chu, Y. Xin, E. S. Choi, H. Zhou, and J. Liu, *Nature Communications* **14** (2023), 10.1038/s41467-023-36886-2.
- ²²³M. Ohno, T. C. Fujita, and M. Kawasaki, *Science Advances* **10** (2024), 10.1126/sciadv.adk6308.
- ²²⁴D. Klimm, C. Gugushev, D. J. Kok, M. Naumann, L. Ackermann, D. Rytz, M. Peltz, K. Dupré, M. D. Neumann, A. Kwasniewski, D. G. Schlom, and M. Bickermann, *Crystengcomm* **19** (2017), 10.1039/c7ce00942a.
- ²²⁵F. Y. Guo, W. H. Zhang, M. Ruan, J. B. Kang, and J. Z. Chen, *Journal of Crystal Growth* **402** (2014), 10.1016/j.jcrysgro.2014.05.011.
- ²²⁶J. Kang, M. Ruan, X. Chen, C. Liu, W. Liu, F. Guo, and J. Chen, *Optical Materials* **36** (2014), 10.1016/j.optmat.2014.03.013.
- ²²⁷J. Kang, W. Xu, X. Chen, W. Liu, F. Guo, S. Wu, and J. Chen, *Journal of Crystal Growth* **395**, 104 (2014).
- ²²⁸M. Ohno, T. C. Fujita, and M. Kawasaki, *Applied Physics Letters* **122** (2023), 10.1063/5.0151959.